



**UNIVERSIDAD DE INVESTIGACIÓN DE
TECNOLOGÍA EXPERIMENTAL YACHAY**

Escuela de Ciencias Físicas y Nanotecnología

**TÍTULO: Numerical Study of Hilltop Inflationary (HI)
Model.**

Trabajo de integración curricular presentado como
requisito para la obtención
del título de Físico

Autor:

Zambrano Jordan

Tutor:

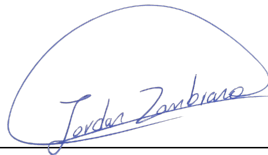
Ph.D Clara Rojas

Urcuquí, Diciembre 2023

AUTORÍA

Yo, **Zambrano Faubla Jordan Alberto**, con cédula de identidad 235020020-6, declaro que las ideas, juicios, valoraciones, interpretaciones, consultas bibliográficas, definiciones y conceptualizaciones expuestas en el presente trabajo; así como, los procedimientos y herramientas utilizadas en la investigación, son de absoluta responsabilidad de el/la autora (a) del trabajo de integración curricular. Así mismo, me acojo a los reglamentos internos de la Universidad de Investigación de Tecnología Experimental Yachay.

Urququí, diciembre 2023.




Jordan Alberto Zambrano Faubla
CI. 235020020-6

AUTORIZACIÓN DE PUBLICACIÓN

Yo, **Zambrano Faubla Jordan Alberto**, con cédula de identidad 235020020-6, cedo a la Universidad de Investigación de Tecnología Experimental Yachay, los derechos de publicación de la presente obra, sin que deba haber un reconocimiento económico por este concepto. Declaro además que el texto del presente trabajo de titulación no podrá ser cedido a ninguna empresa editorial para su publicación u otros fines, sin contar previamente con la autorización escrita de la Universidad.

Asimismo, autorizo a la Universidad que realice la digitalización y publicación de este trabajo de integración curricular en el repositorio virtual, de conformidad a lo dispuesto en el Art. 144 de la Ley Orgánica de Educación Superior

Urcuquí, diciembre 2023.



Jordan Alberto Zambrano Faubla
CI. 235020020-6

Acknowledgements

I would like to express my heartfelt gratitude to Professor Clara Rojas for her unwavering support and invaluable advice throughout our time working together. Her guidance has been instrumental in my growth and learning.

I am also deeply thankful to all my professors at Yachay Tech for their dedication and inspiration. Each of them has played a crucial role in shaping my educational journey and confirming the path I have chosen.

To my beloved family, I owe a debt of gratitude for their unwavering support and the unwavering faith they have placed in me. Finally, I extend my warmest thanks to my friends, who have not only been there for me but have also been a source of incredible learning. Your understanding and friendship have meant the world to me. This journey wouldn't have been the same without all of you, and I am profoundly grateful for your presence in my life.

Resumen

La inflación cósmica fue propuesta para resolver algunos de los problemas llamados "fine-tuning" de la teoría del "Big Bang Caliente", como el problema de la planitud y el problema del horizonte. Este enfoque requiere la selección de un potencial que guíe esta época de inflación. Para este trabajo, se selecciona el modelo Hilltop cuártico, que tiene un parámetro libre cuyo comportamiento afecta directamente los observables obtenidos en este estudio. Se obtienen resultados sobre el espacio sin perturbaciones y un par de características observacionales, como el índice espectral escalar n_s , la razón tensor-escalar r , y el espectro de potencia escalar P_S . Estos resultados se comparan con informes observacionales como el de Planck 2018. Finalmente, se concluye que este modelo es altamente favorecido por los resultados experimentales de Planck y que existe un rango de parámetros para los cuales hay una intersección entre el conjunto de resultados numéricos y observacionales.

Palabras Clave: Cosmología, Inflación, Slow-roll, Espectro de potencia, Potencial Hilltop.

Abstract

Cosmological inflation was proposed to solve some of the fine tuning problems with the Hot Big Bang theory such as flatness and horizon problems. This approach requires the selection of a potential that drives this epoch of inflation. For this work we selected the Hilltop quartic model, that has a range of free parameters which behavior affects directly observables obtained from this work. We use two approaches: slow-roll approximation and numerical calculation. We obtained results for the background and a couple of observational features like: scalar spectral index n_s , tensor-scalar ratio r , and scalar power spectrum P_S . These results are compared to observational reports such as the Planck 2018 results. Finally, we conclude that this model is highly favored by Plank's results and that exists a range of parameters for which there is an intersection between numerical and observational results.

Keywords: Cosmology, Inflation, Slow-roll, Power Spectrum, Hilltop potential.

Contents

List of Figures	xiv
List of Tables	xvi
1 Introduction	1
1.1 Hot Big Bang Theory	2
1.1.1 Horizon Problem	3
1.1.2 Flatness Problem	6
1.2 Problem Statement	7
1.3 General and Specific Objectives	7
2 Methodology	9
2.1 Inflation	9
2.1.1 Inflation Solution for Horizon Problem	10
2.1.2 Inflation Solution for Flatness Problem	10
2.2 Scalar field	11
2.3 Slow Roll	12
2.4 Perturbation Theory	13
2.5 Hilltop Potential	16
3 Results & Discussion	19
3.1 Slow-Roll Parameters	19
3.2 Slow Roll Background Solutions	21
3.3 Slow Roll Perturbations	24
3.4 Numerical Background Solutions	25
3.5 Numerical Perturbation Solutions	26
4 Conclusions & Outlook	33

A Mathematica Code Used	35
Bibliography	47

List of Figures

2.1	Hilltop potential for different values of the parameter μ : $\mu = 18$ (blue), $\mu = 25$ (orange), and $\mu = 30$ (green).	17
3.1	First slow roll parameter against the value of ϕ , for values of $\mu = 1$ (blue) and $\mu = 2$ (orange).	20
3.2	Relation between ϕ_{end} and μ , showing a linear pattern.	21
3.3	Relation between ϕ_{ini} and μ for $N = 60$ (blue), and $N = 50$ (orange).	22
3.4	Relation between free parameter M and μ	23
3.5	Plots of solutions of the background equations of motion under the slow-roll approximation, for scale factor a and inflaton field ϕ , for a fixed value of the parameter $\mu = 20$	23
3.6	Plots of Scalar perturbation spectrum for different values of parameter μ : 20 (blue), 30 (orange), 40 (green), and 50 (red), into the slow roll approximation for $N = 60$	24
3.7	Plots of relation of observable against the parameter μ for $N = 50$ (blue) and $N = 60$ (orange) for slow roll approximation. a) profile of spectral index $n_S(k)$ evaluated at $k = 0.002 \text{ Mpc}^{-1}$ against μ , b) profile of tensor scalar ratio $r(k)$ evaluated at $k = 0.002$ against μ and c) profile of spectral index $n_S(k)$ evaluated at $k = 0.002 \text{ Mpc}^{-1}$ against tensor scalar ratio $r(k)$ evaluated at $k = 0.002 \text{ Mpc}^{-1}$	25
3.8	Plots of numerical solutions (solid) and slow roll (dashed) of the background equations of motion, for scale factor a and inflaton field ϕ , for a fixed value of the parameter $\mu = 20$	26
3.9	Relation of conformal η and cosmic time t for $\mu = 20$ and $N = 60$	27
3.10	Plots of the components of ν_k evaluated at pivot scale $k = 0.05 \text{ Mpc}^{-1}$ for different parameters of the model a) and b) represents real and complex components comparing between $N = 60$ (blue) and $N = 50$ (orange) and with black and brown points representing the point of horizon crossing in each respective case, both with a fixed parameter $\mu = 20$. c) and d) represents real and complex components comparing between two different values of μ : $\mu = 20$ (blue) and $\mu = 30$ (orange). Black and brown points represent the horizon crossing in each case	28
3.11	Comparison of numerical (solid curves) and slow roll (dashed curves) results of $n_S(k)$ and $r(k)$ evaluated at $k = 0.002 \text{ Mpc}^{-1}$, compared for different values of μ , considering $N = 60$ (blue) and $N = 50$ (orange), also it is shown values of observational results obtained by Planks 2018 ¹ (black): $n_S = 0.9649 \pm 0.0042$ and $r < 0.056$	29

3.12	Relation between numerical calculation of $n_S(k)$ vs $r(k)$ evaluated at $k = 0.002 \text{ Mpc}^{-1}$ for different values of μ considering $N = 50$ (orange) and $N = 60$ (blue).	30
3.13	a) Scalar perturbations spectrum from numerical approach against k , b) Log plot of scalar perturbation spectrum, both for $\mu = 20$ (blue), $\mu = 30$ (orange), $\mu = 40$ (green), and $\mu = 50$ (red).c) Comparison between slow roll (dashed) and numerical (solid) result of $P_S(k)$ for $\mu = 20$ (blue) and $\mu = 30$ (orange).	31

List of Tables

3.1	Values of t_{end} for parameter selection $\mu = 20$, for $N = 60$ and $N = 50$	26
-----	---	----

Chapter 1

Introduction

Since the work of Einstein, with the development of the general relativity, a completely new field of study was created. If it is considered the Universe as a whole, then start to appears some interesting features. Friedmann was one of the firsts to propose solutions to the Einstein Field Equations, and with this, opened the road to a new special feature for the universe, solutions obtained by Friedmann gave as result a universe that evolves in time².

One of the main considerations done by Friedmann when he obtained the equations of evolution of the Universe, was that it is homogeneous and isotropic. That it would be homogeneous means that the density of matter will follow a constant distribution, of course this is at large scales, when it considered from a cosmological scale. With this in mind it is unlikely that all the matter that it can be seen from the Earth were just getting apart from the observation point. And isotropic refers to the characteristic that Universe is equal in any direction of observation. This means that no matter where the observational point is set in the whole universe, it will look just the same than any other point.

In the very first years of this consideration there was a real controversy about how evolves the universe. Does it expands?, or is it static? The importance of these questions relies on the justification for the introduction of the cosmological constant, which, according to Einstein, was necessary if one is trying to explain an static universe.

It was until the discovery of Hubble and Lemaitre, at the end of the decade of 20's³, when this discussion reach a solution. They found independently a direct relation between the velocity at which a galaxy moves from the earth and the distance at which it is located⁴, this relation is known as the Hubble parameter. The universe expands and it does in a very important and intriguing way. With this in mind, not much time passed before the idea of expansion appeared. Taking into consideration the arrow of time, Lemaitre postulate another idea: what if all the things that we know comes from one single point? A point as the origin of all the universe⁵, this was later called the Big Bang theory.

This approach is also refereed to as Hot Big Bang Theory because it takes the origin of the universe as a hot and very dense singularity point from which all the universe evolves. The main problems with Hot Big bang theory are related to how likely the conditions needed are to result in the current universe, given the measurements that have been made about how it evolves. This situation results in a fine tuning selection of circumstances. The two problems

that are most mentioned in literature are the horizon problem, and the flatness problem.

1.1 Hot Big Bang Theory

To better understand the aim of this work, it is necessary to recover some of the most fundamental aspects of the framework in which inflation appears. Hence, some concepts with significant importance in the development of the classical Big Bang theory or Hot Big Bang theory will be reviewed. The first thing that is necessary to comprehend is that the "Big Bang Theory" is a theory that does not explain why the universe emerged. Additionally, this theory does not explain in detail the conditions and characteristics of the explosion to which the term "Big Bang" makes reference. Instead, it is a theory that allows us to calculate and to understand what happened after this moment.

Recovering the idea of the cosmological principle, homogeneity and isotropicness of the universe at large scales can be expressed through the Friedmann-Robertson-Walker (FRW) metric^{6,7,8}.

$$ds^2 = -dt^2 + a^2(t) \left[\frac{dr^2}{1 - kr^2} + r^2(d\theta^2 + \sin^2\theta d\phi^2) \right]. \quad (1.1)$$

Where $a(t)$ is the scale factor, and k is the term that refers the curvature parameter and can take values of $k = -1$, $k = 0$, and $k = +1$, for negatively curved, flat curved and positively curved, respectively⁹. These curvature shapes are related to specific kind of geometry: hyper spherical, euclidean and spherical geometry, respectively¹⁰. Also, this line element is written in polar coordinates form (t, r, θ, ϕ) . In order to deal with this metric, it is necessary to use the Einstein Field equations:

$$G_{\mu\nu} = 8\pi G T_{\mu\nu}. \quad (1.2)$$

Where G is Newton's gravitational constant, and the term $T_{\mu\nu}$ is the energy-momentum tensor. Also, the term $G_{\mu\nu}$ refers to the Einstein tensor:

$$G_{\mu\nu} = R_{\mu\nu} - \frac{1}{2} R g_{\mu\nu}. \quad (1.3)$$

With the term $R_{\mu\nu}$ for the Ricci Tensor, R as the Ricci Scalar and $g_{\mu\nu}$ the metric. $T_{\mu\nu}$ includes properties of the relativistic fluid considered to model the universe¹¹. In this case, it is a perfect fluid; in that way the tensor is expressed as:

$$T_{\mu}^{\nu} = \begin{pmatrix} -\rho(t) & 0 & 0 & 0 \\ 0 & p(t) & 0 & 0 \\ 0 & 0 & p(t) & 0 \\ 0 & 0 & 0 & p(t) \end{pmatrix}. \quad (1.4)$$

This perfect fluid is considered with features: energy density $\rho(t)$ and pressure $p(t)$, which are related through the equation of state:

$$p(t) = w\rho(t). \quad (1.5)$$

With this in mind, depending on the composition of the universe the value of the equation of state coefficient w will change, for example for radiation dominated universe $w = 1/3$ ¹², and for a matter dominated universe $w = 0$ ¹³.

Solving for the FRW metric and replacing non zero terms of the Ricci and Einstein tensor into Eq. 1.2, two equations are obtained, one for solving the time-time components and the other for space-space terms¹⁴. The first one is the Friedmann Equation.

$$\left(\frac{\dot{a}}{a}\right)^2 + \frac{k}{a^2} = \frac{8\pi G}{3}\rho. \quad (1.6)$$

Where a is the scale factor. For the case of flat universe, Friedmann equation is reduced to:

$$\left(\frac{\dot{a}}{a}\right)^2 = \frac{8\pi G}{3}\rho. \quad (1.7)$$

The second expression is an intermediate step¹⁴:

$$2\frac{\ddot{a}}{a} + \left(\frac{\dot{a}}{a}\right)^2 + \frac{k}{a^2} = -8\pi Gp, \quad (1.8)$$

from which can be obtained the acceleration equation¹⁵:

$$\frac{\ddot{a}}{a} = -\frac{4\pi G}{3}(\rho + 3p). \quad (1.9)$$

Also from the momentum conservation law $\nabla^\mu T_{\mu\alpha} = 0$, the expression for the energy conservation is obtained, relating the terms of the derivative of the energy density, pressure and energy density¹⁰:

$$\dot{\rho} + 3\frac{\dot{a}}{a}(p + \rho) = 0. \quad (1.10)$$

1.1.1 Horizon Problem

The horizon problem refers to the limits of causality at the recombination epoch¹⁶. What if two points were causally disconnected at that time? How should that affect the homogeneity of the universe? The comoving distance for the travel of interaction before Cosmic Microwave Background was created, is according to calculation $\sim 180\Omega_0^{-1/2}h^{-1} \text{Mpc}^{-1}$. If this value is compared with the comoving distance that radiation travels after decoupling, which is $\sim 5800h^{-1} \text{Mpc}^{-1}$, the first one is considerable smaller¹⁷.

This would mean that the possibility of a causal connection of different point separated by a greater distance than the Hubble radius should not be possible. At least before of this epoch, those regions were closer, so they could be causally connected. Then, how it is possible that measurements indicate that the thermal black body spectrum is highly homogeneous around the temperature of $T = 2.7 \pm 10^{-5} \text{K}$ ¹⁸.

This problem is better explained when the angular diameter of the horizon at the epoch of recombination, seen by an observer today, is calculated. In that way, it is possible to realize the level of fine-tuning needed to accomplish these conditions.

Following the calculation done by Martin¹⁹, it is calculated the relation between the size of the horizon at the last scattering and the present angular distance to the last scattering.

$$\Delta\Omega = \frac{d_H(t_s)}{d_A(t_s)}, \quad (1.11)$$

where $d_H(t_{ls})$ represents the size of the horizon evaluated at epoch of last scattering, and $d_A(t_{ls})$ is the present angular distance to the last scattering moment. Now, it is explained how to obtained these two quantities.

For this, a special coordinate systems is considered, one in which the origin is on Earth. Then a photon could be emitted from spacial comoving coordinates $(r_{em}, \theta_{em}, \psi_{em})$, but in this case using cosmic time t_{em} . Due to the solution to the geodesic equation, it is known that the calculation of the path followed by the emitted photon can be chosen in a way that coordinates θ and ψ keeps constant. As a consequence, the path can be characterized by the coordinate r , that will be a function of time, $r(t)$.

$$r(t) = r_{em} - \int_{t_{em}}^t \frac{d\tau}{a(\tau)}. \quad (1.12)$$

Then, it is necessary to obtain an expression for the proper distance from the position of the emitted photon at time t to the origin. This quantity is what is called the size of the horizon at time $t = t_{rec}$, a given reception time.

$$d_p(t) = a(t) \left[r_{em} - \int_{t_{em}}^t \frac{d\tau}{a(\tau)} \right]. \quad (1.13)$$

The comoving coordinate of emission is obtained when this value $d_p(t_{rec}) = 0$. Then:

$$r_{em} = \int_0^{t_{rec}} \frac{d\tau}{a(\tau)}. \quad (1.14)$$

Having this, it can be written the distance to the horizon at time $t = t_{rec}$. And consider that it can be taken at any time like $t = t_{ls}$, then we have the first term for our expression of $\Delta\Omega$.

$$d_H(t_{rec}) = a(t_{rec})r_{em}. \quad (1.15)$$

Now, for the second, it is considered the distance from a point where is emitted a photon at time $t = t_{em}$ that arrives to the earth right now.

$$r_{em} = \int_{t_{em}}^{t_0} \frac{d\tau}{a(\tau)}. \quad (1.16)$$

This value is used to calculate d_A :

$$d_A = a(t_{em})r_{em}. \quad (1.17)$$

For this expression it is evaluated again at $t = t_{ls}$:

$$d_A(t_{ls}) = a(t_{ls})r_{em}. \quad (1.18)$$

After this:

$$\Delta\Omega = \left[\int_0^{t_{ls}} \frac{d\tau}{a(\tau)} \right] \times \left[\int_{t_{ls}}^{t_0} \frac{d\tau}{a(\tau)} \right]^{-1}. \quad (1.19)$$

where the terms $a(t_{ls})$ are cancelled out, and the expression just relates the term r_{em} .

The next step is to consider an expression for the quantity $a(t)$ and evaluate it in the equation above. Hence, Martin¹⁹ makes the assumption of a universe that is radiation-dominated before the recombination epoch and after that is matter-dominated. Under this approach the epoch dominated by radiation is interrupted $t_i < t < t_{\text{end}}$ during which inflation occurs, when appears the effect of and unknown fluid X , that follows a fixed equation of state that keeps constant with the parameter ω_x .

Then it is used the following piece-wise function, that is continuous and it is also its first derivative.

$$a(t) = \begin{cases} a_i(2H_i t)^{1/2} & , 0 \leq t < t_i \\ a_i \left[\frac{3}{2}(1 + \omega_x)H_i(t - t_i) + 1 \right]^{\frac{2}{3(1+\omega_x)}} & , t_i \leq t < t_{\text{end}} \\ a_{\text{end}} [2H_{\text{end}}(t - t_{\text{end}} + 1)]^{1/2} & , t_{\text{end}} \leq t < t_{\text{eq}} \\ a_{\text{eq}} \left[\frac{3H_{\text{eq}}}{2}(t - t_{\text{eq}}) + 1 \right]^{2/3} & , t_{\text{eq}} \leq t < t_0 \end{cases} . \quad (1.20)$$

where the subscript eq in parameters refers to the epoch of equilibrium, when the density of radiation and the density of matter become comparable, in the middle time between the epoch of the dominance of radiation and matter.

Then evaluating in expressions above, Eq. 1.15 and Eq. 1.18, it is obtained.

$$d_A(t_{\text{ls}}) = a_{\text{ls}} \int_{t_{\text{ls}}}^{t_0} \frac{d\tau}{a(\tau)}, \quad (1.21)$$

$$= a_{\text{ls}} \frac{2}{a_0 H_0} \left[1 - \left(\frac{a_{\text{ls}}}{a_0} \right)^{1/2} \right], \quad (1.22)$$

$$d_H(t_{\text{ls}}) = a_{\text{ls}} \int_0^{t_{\text{ls}}} \frac{d\tau}{a(\tau)}, \quad (1.23)$$

$$= a_{\text{ls}} \frac{1}{a_0 H_0} \left(\frac{a_{\text{ls}}}{a_0} \right)^{1/2} \left\{ 1 + \frac{1 - 3\omega_x}{1 + 3\omega_x} \frac{a_{\text{end}}}{a_{\text{ls}}} \left[1 - \left(\frac{a_i}{a_{\text{end}}} \right)^{\frac{(1+3\omega_x)}{2}} \right] \right\}. \quad (1.24)$$

The final expression, which is obtained evaluating Eq. 1.22, and Eq. 1.24, into the Eq. 1.11.

$$\Delta\Omega = \frac{1}{2} \left[1 - (1 + z_{\text{ls}})^{-1/2} \right]^{-1} (1 + z_{\text{ls}})^{-1/2} \left\{ 1 + \frac{1 - \omega_x}{1 + 3\omega_x} \frac{1 + z_{\text{ls}}}{1 + z_{\text{end}}} \left[1 - e^{-N(1+3\omega_x)/2} \right] \right\}. \quad (1.25)$$

where $N \equiv \ln(a_{\text{end}}/a_{\text{ini}})$ refers of the number of e-foldings, which represents the times the universe has increases their size when it has been inflated or in other words the amount of inflation. For this case, it will be taken $N = 0$, the case of no inflation. Then, the expression approximates as:

$$\Delta\Omega \approx 0.5(1 + z_{\text{ls}})^{-1/2} \approx 0.85^\circ. \quad (1.26)$$

What this calculation reveals is that the angular diameter of causal connected space at that time is less than 1° ¹⁹. The sky would be full of patches of that angular diameter with different properties between them, making the homogeneity between them improbable. This situation and the fact that it is not seen in this way from observations what carries the thoughts to the called horizon paradox problem. In next sections it will be discussed how inflation solves this paradox.

1.1.2 Flatness Problem

The flatness problem comes from other fine-tuning situation, one that relates to the geometry of the universe and energy density in it. As a result, it is seen the universe as extremely flat. The problem comes when it is noticed that this situation is highly unlikely¹⁶. To better understand this problem, it is useful to use the definition of density parameter Ω .

$$\Omega \equiv \frac{\rho}{\rho_{\text{cri}}}. \quad (1.27)$$

where ρ represents the energy density and ρ_{cri} represents its critical value, that marks the value for which the universe would be completely flat¹⁹. That follows the expression:

$$\rho_{\text{cri}}(t) = \frac{3H^2}{8\pi G}. \quad (1.28)$$

The measurement value of this parameter is currently obtained in the range $0.995 < \Omega_0 < 1.005$ ²⁰, showing that our universe is very close to being flat. Considering this definition, it will be used the Friedmann equation, which will be developed in the following chapter, in the form:

$$|\Omega_{\text{tot}}(t) - 1| = \frac{|k|}{a^2 H^2}. \quad (1.29)$$

Where Ω_{tot} represents the sum over all the kind of matter that exist in the universe. Also what can be obtained from the equation above is the relation of the curvature term k and the energy density term Ω_{tot} as well as their evolution on time¹⁴.

For the case where $\Omega_{\text{tot}} = 1$, it is found that the term of curvature has to maintain the value $k = 0$, this means that if the universe is flat, it will keep flat. Otherwise, the density parameter will change with time¹¹. If it is analyzed more deeply, it is found that the relation of the term $a^2 H^2$ evolve in some way with time depending of the dominance of matter in the universe.

$$\begin{aligned} a^2 H^2 &\propto t^{-1} && \text{radiation dominated time;} \\ a^2 H^2 &\propto t^{-2/3} && \text{matter dominated time;} \end{aligned} \quad (1.30)$$

Then using the relation of the Friedmann equation, Eq. 2.18, they becomes:

$$\begin{aligned} |\Omega_{\text{tot}} - 1| &\propto t^1 && \text{radiation dominated time;} \\ |\Omega_{\text{tot}} - 1| &\propto t^{2/3} && \text{matter dominated time;} \end{aligned} \quad (1.31)$$

As can be seen, the difference between the density parameter Ω_{tot} and unity is a functions that increase as the age of the universe evolves. This means that the situation of exact flatness is an unstable state¹⁴. If, at some point, the density parameter deviates significantly from 1, then it will get more and more different. If this parameter is grater than 1, it would evolve increasing this value until the universe collapse due to gravity, this is the close model universe. And if the parameter is less than 1 then the gravitational attraction would become weaker and weaker, carrying the expansion rate asymptotically to a constant, this is the open universe model²¹. This means that in order to have at this epoch a density parameter so close to 1, at early age of the universe this value had to be extremely

close to the unity. If it is taken, for example, the time of nucleosynthesis, approximately $1s$ after the Big Bang, it is required¹¹:

$$|\Omega_{\text{tot}}(t_{\text{nuc}}) - 1| \lesssim 10^{-16}. \quad (1.32)$$

The fine-tuning problem comes when it is analyzed how unlikely is that this value is so small. In next chapter it will be explained how inflation solves this puzzle.

1.2 Problem Statement

Considering these puzzles, it was necessary a mechanism to explain why the universe starts with those so unlikely conditions. Before inflation, there were consider as curiosities, and working on Big Bang theory relied on making these assumptions. In that way, inflation explains and establishes causal relations for the conditions needed to the formation of the universe. The flatness and horizon problems are just a couple of the issues that inflation solved; it also helped to better understand the formation of large scale structure of the universe and the heterogeneity of the Comic Microwave Background (CMB) temperature spectrum. In next chapter, it will be discussed further the mechanism and definition of the inflation theory.

In the field of inflation research, one of the main branches involves the analysis of different inflation potentials. For this purpose there have been developed several models that tries to explain features of the early universe and consequences that can be seen from this epoch. The way in which these potentials are studied and contrasted with observations is mainly through perturbation theory. This involves perturbing the usual metric of the universe, a concept that will be explained in more detail later. From this analysis there are obtained scalar and tensor perturbation spectrum, which serve as observables for cosmological experiments conducted in projects like COBE or Planck¹.

It is also important to consider that Planck Collaboration is not the only work dedicated to make measurements about inflation. For example BICEP/Keck Collaborations that measure the polarization of the CMB specifically for the B-modes, and whose last results shows a new constraint for tensor-scalar ratio $r < 0.036$ in the 95% CL.²² While experiments like Atacama Cosmology Telescope has observed some results that creates a tension with the ones reported by Planck satellite. This "CMB tension" has been measured in the range 1.8σ to 3.5σ depending of the extended model, starting from the Λ CDM baseline²³.

The comparison between observational parameters and observables obtained from the study of potentials allows the constraining of certain models and the rejection of others when the data is sufficiently accurate. In this work, it is taken one of this potentials, the Hilltop model, which is developed with more detail later.

1.3 General and Specific Objectives

This work is divided into three chapters. In the first one, an introduction to the work is provided, where is explained some of the basic concepts necessary to understand further analysis. Also, certain features of the Hot Big Bang Theory are discussed, along with some of its puzzles or fine-tuning problems that eventually lead to the development of the inflationary theory. In the second chapter, the theoretical basis used for this work is explained in more

detail. Inflation and perturbation theory are elaborated upon, along with all the numerical aspects considered for the computational approach of this work. Third chapter is about results, they are separated in background calculation and perturbation calculations. The approach used for the analysis, both numerical and slow roll, is discussed as well. Finally in the conclusion chapter, a summary of the topics developed in this work is provided, along with the final insights obtained from the analysis of the Hilltop model.

Einstein summation convention is used for this work. As usual, greek indices runs from 0 to 3 and latin indices from 1 to 3. The signature of the metric is $(-, +, +, +)$. Also values as \hbar and c are taken as 1.

Chapter 2

Methodology

2.1 Inflation

In 1981 Alan Guth proposed the idea of inflation in an attempt to solve some problems with the "Hot Big Bang Theory": horizon and flatness are some of them¹⁶. Inflation refers to a period of rapidly expansion for the universe placed after the beginning of the time refereed by Big Bang. This expansion would follow an exponential behavior. Mathematically this fact about expansion is described as¹⁴:

$$\ddot{a}(t) > 0. \quad (2.1)$$

With this condition in mind, it can be evaluated in acceleration equation, Eq. 1.9, which tells:

$$\rho + 3p < 0, \quad (2.2)$$

as a consequence. Then as the energy density is considered as a positive number, it results:

$$p < -\frac{\rho}{3}. \quad (2.3)$$

For inflation to occurs it is necessary a negative pressure exotic matter. The condition described in Eq. 2.1 can be described also in the following way:

$$\frac{d}{dt} \frac{H^{-1}}{a} < 0. \quad (2.4)$$

Where the term $\frac{H^{-1}}{a}$ is the Hubble length, which for occurring inflation has to be a decreasing value in time. Other way to see this condition is:

$$-\frac{\dot{H}}{H^2} < 1, \quad (2.5)$$

that tells that for inflation era, H varies slowly on Hubble timescale. Also notice that if $\dot{H} \ll H^2$, H would be almost constant and it would result in an almost exponential expansion $a \propto e^{Ht}$ ¹¹.

Now it will be developed how inflation solves horizon and flatness problems from the classic Big Bang theory.

2.1.1 Inflation Solution for Horizon Problem

For solving the horizon problem, it is necessary to consider Eq. 1.25 and how the term N that relates the amount of inflation with the size of the horizon at the time of last scattering. The condition for solving this problem can be written as $\Delta\Omega > 4\pi$ that refers to obtaining a last scattering surface very isotropic¹⁹, in that way can be explained the lack of expected heterogeneity. This condition is used as constrain to obtain:

$$N \gtrsim -4 + \ln z_{\text{end}}. \quad (2.6)$$

This result shows that exist a number of e-foldings for which the condition to solve the horizon problem is met. Considering that redshift at the end of inflation, z_{end} , is in the order of $\sim 10^{26}$ ²⁴, then the number of e-foldings:

$$N \gtrsim 55 \quad (2.7)$$

2.1.2 Inflation Solution for Flatness Problem

For solving the flatness problem thought the way of inflation it is necessary to consider that for the epoch at which it occurred, the redshift has to be $z \gg z_{\text{end}}$, and for this time it is considered that the universe is full with some exotic unknown matter, different from usual matter or radiation, that will be refered as X , characterized by the equation of state ω_X . This equation of state can be chosen in a way that allows that $\Omega_T - 1$ be close to zero¹⁹. Also for this purpose it is useful to write Ω_T in function of the scale factor $a(t)$ ¹⁹, then it is obtained

$$\Omega_T(a) = \sum_{i=1}^N \Omega_i(t_0) \left(\frac{a}{a_0}\right)^{-3(1+\omega_i)} \left\{ \sum_{j=1}^N \Omega_j(t_0) \left(\frac{a}{a_0}\right)^{-3(1+\omega_j)} - [\Omega_T(t_0) - 1] \left(\frac{a}{a_0}\right)^{-2} \right\}^{-1}. \quad (2.8)$$

Considering that for inflation it is necessary to deal with this unknown matter, it is useful to write Ω_T in relation with the density parameter of this new matter Ω_X

$$\Omega_T = \frac{\Omega_X(a_i)}{\Omega_X(a_i) + [1 - \Omega_T(a_i)] \left(\frac{a}{a_i}\right)^{1+3\omega_X}}. \quad (2.9)$$

At the time of the end the the inflation the value of the scale factor $a(t_{\text{end}})$ makes this expression above tend to 1 when the condition $1 + 3\omega_X$ is fulfilled, this situation is maintained for all the time the matter X dominates. This is the mathematical description of negative pressure material, necessary for inflation.

It is possible also, to obtain information about the amount of inflation needed to solve the flatness problem. For that it is necessary to look for the value of N that could carry Ω_T very close to the unity at the end of inflation, so that, it still maintain considerable close to one still after radiation and matter domination on the universe.

$$\left(\frac{a_{\text{end}}}{a_i}\right)^{1+3\omega_X} = e^{N(1+3\omega_X)} \lesssim 10^4 \times z_{\text{end}}^{-2}, \quad (2.10)$$

which can be expressed as:

$$N \gtrsim -4 + \ln z_{\text{end}}. \quad (2.11)$$

This is the same condition obtained from the solution to the horizon problem.

2.2 Scalar field

Going further in inflation propose, it is necessary to consider that if happened, it was at a very early time in the universe. This implies that this process occurred a very high energies, then the better way we can understand a process like this is with quantum field theory resources. In fundamental physics features of any system can be specified using the Lagrangian expression, that is used to define the action:

$$S = \int_{-\infty}^{\infty} L dt, \quad (2.12)$$

where L refers to Lagrangian. L depends of the degrees of freedom of the system, in that sense it is considered a finite system, with finite number of particles, and finite number of coordinates. But when it is tried to specify the behavior of a system with infinity degrees of freedom, because in the field sense this exist everywhere, it is necessary to change the formulation. In that way appears the definition of Lagrangian density \mathcal{L}

$$L = \int \mathcal{L} d^3 r, \quad (2.13)$$

that is a Lorentz invariant quantity, and has units of $[energy]^4$. \mathcal{L} is a function that depends on the fields, that are defined, as well as on their derivatives respect to space and time. In a significant portion of the literature, a specific kind of model is considered, employing a scalar field formulation¹⁷, where 'scalar' denotes a field with spin-0, similar to the Higgs boson.

Considering the term of the action that contains only the scalar field ϕ , that is taken as decoupled from other fields where $V(\phi)$ refers to some free function, a potential that is constrained after for having some properties, and the first term is known as kinetic term. Then if it is used relativistic index notation, where coordinates are expressed as $x^\mu \equiv (t, \mathbf{r}) \equiv (x^0, x^i)$, the relation of action would be¹⁹:

$$S = - \int d^4 x \sqrt{-g} \left[\frac{1}{2} g^{\mu\nu} \partial_\mu \phi \partial_\nu \phi + V(\phi) \right]. \quad (2.14)$$

Where g is the determinant of the metric tensor. This action describes a universe driven by a scalar field, $\phi(t, x)$, that depends on time and position. However, as will be shown, due to symmetry of stress-energy tensor, it will depend only on time $\phi(t)$. This field is called inflation²⁵. The stress energy tensor can be obtained from Noether's theorem or from the calculation of the action of scalar field^{17 25}. And it is expressed in the following way:

$$T_{\mu\nu} = \partial_\mu \phi \partial_\nu \phi - g_{\mu\nu} \left[\frac{1}{2} g^{\alpha\beta} \partial_\alpha \phi \partial_\beta \phi - V(\phi) \right]. \quad (2.15)$$

It is obtained from time-time component of stress-energy tensor $T_0^0 = \rho$ that:

$$\rho = \frac{1}{2}\dot{\phi}^2 + V(\phi). \quad (2.16)$$

Considering that developing the space-space component $T_j^i = -p\delta_j^i$, and the total energy density ρ is the sum of kinetic and potential terms, then:

$$p = \frac{1}{2}\dot{\phi}^2 - V(\phi). \quad (2.17)$$

Having this relations it is possible to evaluate Friedmann and energy conservation equations, Eq. 1.7 and Eq. 1.10, respectively, with the pressure and energy density terms. From them it is obtained:

$$H^2 = \frac{1}{3} \left[\frac{1}{2}\dot{\phi}^2 + V(\phi) \right], \quad (2.18)$$

$$\ddot{\phi} + 3H\dot{\phi} + V' = 0, \quad (2.19)$$

where V' represents the derivative of the potential respect of the field ϕ . The first equation is known as the Friedmann equation and the second Klein-Gordon equation²⁵. These pair of expressions are called the equations of motion of a scalar field driven universe.

2.3 Slow Roll

Having this set of equations it is possible to select a given potential and solve Friedmann and Klein-Gordon equations in order to obtain the evolution of the field $\phi(t)$ and scale factor $a(t)$. But it is useful to approximate these equations in order to make the process of solving less complex. If it consider the case when potential energy $V(\phi)$ dominates over the kinetic energy, then is obtained the called slow roll approximation.

Notice also that Eq. 2.19 looks like a harmonic oscillator equation, with a friction term proportional to the Hubble parameter H . For that case it is known that for large values of the friction term the system will be damped making the acceleration term $\ddot{\phi}$ negligible²⁶. Mathematically this will approximate Eq. 2.18 and Eq. 2.19 to the following expressions:

$$H^2 \simeq \frac{1}{3}V(\phi), \quad (2.20)$$

$$3H\dot{\phi} \simeq -V_{\phi}. \quad (2.21)$$

For slow roll approach there are defined some parameters that give features and let to know if conditions of inflation are been accomplished. Mainly there are two kinds: the first one are defined of function of the Hubble parameter, they are also called Hubble flow parameters, which characterise the way Hubble parameters evolve in time²⁷. These are defined in the following way:

$$\epsilon_H(\phi) = \left[\frac{H'(\phi)}{H(\phi)} \right]^2, \quad (2.22)$$

$$\eta_H(\phi) = \frac{H''(\phi)}{H(\phi)}. \quad (2.23)$$

Also slow roll parameters can be defined in function of the potential selected for the model of inflation^{28,29}:

$$\epsilon_V(\phi) = \frac{1}{2} \left[\frac{V'(\phi)}{V(\phi)} \right]^2, \quad (2.24)$$

$$\eta_V(\phi) = \frac{V''(\phi)}{V(\phi)}. \quad (2.25)$$

These last equations requires not only the potential of inflation but also the information about how it evolves. For this work are used both approaches, the second one is used in order to obtain values of the field at the end of inflation. And the first approach is used for the calculation of the observables quantities under the slow roll paradigm. Conditions for inflation in terms of these parameters are³⁰:

$$\epsilon(\phi) < 1, \quad (2.26)$$

$$|\eta(\phi)| < 1. \quad (2.27)$$

That is why for defining the end of inflation it is used the situation when one of those conditions are broken³¹, then:

$$\epsilon(\phi_{\text{end}}) = 1, \quad (2.28)$$

$$|\eta(\phi_{\text{end}})| = 1. \quad (2.29)$$

In next sections, it will be discussed about mentioned observable quantities and how are they obtained from perturbations theory and how slow roll can be used to compute them.

2.4 Perturbation Theory

After studying background solutions for the inflationary epoch, it is studied perturbations created during that time. This is done in order to understand how these perturbations become inhomogeneities, leading to the formation of large-scale structure of the Universe that can be observed today. The basic idea of this is that there were some primordial perturbations that grow up and increase their amplitude because of gravitational instabilities, then as a consequence all the structures in the universe take form³².

To study these perturbations there is developed cosmological perturbation theory that tries to study the origin and evolution of small perturbations from homogeneity and isotropic solutions¹⁷. For that, there are considered three kind of perturbations: scalar, vector, and tensor ones, but for inflation the effect of vector perturbation is neglected because they are no caused by inflation²⁸.

The way this analysis is by done is considering coupled linear differential equations for each kind of perturbations, in that way, ones can be studied while the effect of the other are not taken into account. This treatment also let to study perturbations separately from background solutions. With that aim, gauge variables³³ and perturbations are defined in order to obtain a situation where, in the absence of perturbations the system will return to usual background state¹⁷.

In that way, it will be considered a perturbed FRW metric for a flat universe under the longitudinal gauge³². Whose line element is given by:

$$ds^2 = -[1 + 2\Phi(t, x)] dt^2 + a^2 [1 - 2\Psi(t, x)] \delta_{ij} dx^i dx^j, \quad (2.30)$$

where $\Phi(t, x)$ and $\Psi(t, x)$ are the gauge invariant variables. Then for obtaining equation of perturbations it is necessary to solve Einstein's equation for this perturbed metric:

$$\delta G_{\nu}^{\mu} \equiv \delta R_{\nu}^{\mu} - \frac{1}{2} \delta_{\nu}^{\mu} \delta \mathcal{R} = 8\pi G \delta T_{\nu}^{\mu}, \quad (2.31)$$

where $\delta G_{\nu\mu}$ represent the perturbed Einstein tensor, δR_{ν}^{μ} is the perturbed Ricci tensor, $\delta \mathcal{R}$ is the perturbed Ricci scalar, and δT_{ν}^{μ} the perturbed stress-energy tensor. Then the metric that is considered is the following:

$$g_{\mu\nu} = \begin{pmatrix} -1 - 2\Phi(t, x) & 0 & 0 & 0 \\ 0 & a^2 [1 - 2\Psi(t, x)] & 0 & 0 \\ 0 & 0 & a^2 [1 - 2\Psi(t, x)] & 0 \\ 0 & 0 & 0 & a^2 [1 - 2\Psi(t, x)] \end{pmatrix}. \quad (2.32)$$

Having that this metric is a diagonal matrix, the contravariant metric would be given by the inverse of each of the components.

$$g^{00} = -\frac{1}{1 + 2\Phi}, \quad (2.33)$$

$$g^{ii} = \frac{1}{a^2(1 - 2\Psi)}, \quad (2.34)$$

expressions that can be approximated considering that Ψ and Φ are small:

$$g^{00} = -1 + 2\Phi, \quad (2.35)$$

$$g^{ii} = \frac{1}{a^2}(1 + 2\Psi). \quad (2.36)$$

Tapia and Rojas³² developed this calculation explicitly, computing perturbed quantities of the Einstein tensor G_{ν}^{μ} and stress-energy tensor T_{ν}^{μ} up to first order and they were obtained the following set of equations:

$$\nabla^2 \Phi - 3\mathcal{H}\Phi' - (\mathcal{H}' + 2\mathcal{H}^2)\Phi = \frac{3}{2}l^2 (\varphi'_0 \delta\varphi' + V_{\phi} a^2 \delta\varphi), \quad (2.37)$$

$$\Phi' + \mathcal{H}\Phi = \frac{3}{2}l^2 \varphi'_0 \delta\varphi, \quad (2.38)$$

$$\Phi'' + 3\mathcal{H}\Phi' + (\mathcal{H}' + 2\mathcal{H}^2)\Phi = \frac{3}{2}l^2 (\varphi'_0 \delta\varphi' - V_{\phi} a^2 \delta\varphi), \quad (2.39)$$

where $\mathcal{H} = \frac{a'}{a}$, and its relation with H is $H = \mathcal{H}/a$, and the terms φ_0 and $\delta\varphi$ are part of the definition of the perturbed inflaton field:

$$\varphi(t, x) = \varphi_0(t) + \delta\varphi(t, x), \quad (2.40)$$

with φ_0 as the background field, and $\delta\varphi$ is the linear perturbation. Also the term V_{ϕ} represents the derivative of the potential with respect to the inflaton field.

After combining perturbation equations described above, the following expression results:

$$\Phi'' - \nabla^2 \Phi + 2 \left(\frac{a}{\varphi'_0} \right)' \left(\frac{a}{\varphi'_0} \right)^{-1} \Phi' + 2\varphi'_0 \left(\frac{\mathcal{H}}{\varphi'_0} \right)' \Phi = 0, \quad (2.41)$$

or,

$$\sigma'' - \nabla^2 \sigma - z_s \left(\frac{1}{z_s} \right)'' \sigma = 0. \quad (2.42)$$

Considering for this last expression the following definitions: $\sigma = (a/\varphi'_0)$, and $z_s = (a\varphi'_0)/\mathcal{H}$. This equation describes the evolution of perturbations in a classical way, and is used for the situation when perturbations have crossed the horizon. Then, in order to understand dynamics of perturbations before the horizon crossing, it is necessary to use to quantize term, this procedure is developed by Deruelle³⁴. It is defined the gauge invariant variable:

$$u = a \left[\delta\varphi + \frac{\varphi\Phi}{\mathcal{H}} \right], \quad (2.43)$$

which is related to σ in the way:

$$u = \frac{2}{3l^2} \left(\sigma' + \frac{z'_s}{z_s} \sigma \right), \quad (2.44)$$

then using Eq. 2.42 it can be obtained:

$$\nabla^2 \sigma = \frac{3}{2} l^2 z_s \left(\frac{u}{z_s} \right)'. \quad (2.45)$$

Finally, this equation can be expressed as:

$$u'' - \nabla^2 u - \frac{z''_s}{z_s} u = 0, \quad (2.46)$$

that after a Fourier transformation is obtained in function of the mode v_k , where k is the wave number:

$$u''_k + \left(k^2 - \frac{z''_s}{z_s} \right) u_k = 0, \quad (2.47)$$

that is also known as the Mukhanov-Sasaki equation³⁵. According to Tapia³⁶, for modeling the behavior of perturbations can be used separate expressions, one for scalar and the other for tensor ones. Eq. 2.47 is the expression for scalar perturbation dynamics and the following expression correspond to the tensor case³⁷:

$$v''_k + \left(k^2 - \frac{a''}{a} \right) v_k = 0. \quad (2.48)$$

From the solution for these differential equations, there are obtained the modes u_k and v_k , that are used for the definition of cosmological observables. There will be defined power spectra of scalar and tensor perturbations³⁸:

$$P_S(k) = \lim_{kt \rightarrow \infty} \frac{k^3}{2\pi^2} \left| \frac{u_k(t)}{z_s(t)} \right|^2, \quad (2.49)$$

$$P_T(k) = \lim_{kt \rightarrow \infty} \frac{k^3}{2\pi^2} \left| \frac{v_k(t)}{a(t)} \right|^2, \quad (2.50)$$

and with these quantities comes another that is in the same way useful in the process of constraining inflation models, the tensor-scalar ratio³⁷ r :

$$r(k) = 8 \frac{P_T(k)}{P_S(k)}. \quad (2.51)$$

In the same way are defined spectral indices for scalar and tensor perturbations³⁷:

$$n_S(k) = 1 + \frac{d \ln P_S}{d \ln k}, \quad (2.52)$$

$$n_T(k) = \frac{d \ln P_T}{d \ln k}. \quad (2.53)$$

But there is another approach for obtaining the expression for the value of $P_S(k)$, it is usually used when treating with observational data or when research is not biased by a selection of a potential. This is used as a generic function that tries to model and fit the shape of the scalar spectrum as a power law³⁹:

$$\log P_S(k) = \log A_S + (n_S - 1) \log \left(\frac{k}{k_*} \right) + \frac{1}{2} \alpha_S \log^2 \left(\frac{k}{k_*} \right) + \dots, \quad (2.54)$$

where A_S is the amplitude of the spectrum, α_S is the running parameter and k_* is the pivot scale. In the same way there exist an expression for the tensor spectrum¹:

$$\log P_T(k) = \log r A_S + n_T \log \left(\frac{k}{k_*} \right) + \dots, \quad (2.55)$$

2.5 Hilltop Potential

The mathematical expression for the Hilltop model of inflation is given by⁴⁰:

$$V(\phi) = M^4 \left[1 - \left(\frac{\phi}{\mu} \right)^p \right], \quad (2.56)$$

where M is the normalization term, p is the power index and for this work it will be set on $p = 4$, because this model has been more favored by the Planck results¹, and finally the term μ is the parameter associated to the Planck mass. Parameter p has to fulfil the condition $p > 0$ and μ can take any value⁴⁰, but has to be accomplish also the condition for small field limit $\phi < \mu$. This model is also called small field inflation. It appears in a great variety of proposes, in superstring theories and non-linear sigma theories. The shape of the potential, seen in Fig. 2.1, is selected in order to have a very flat potential at the begging of inflation, allowing for a slow roll phase where the potential term is considerably greater than the kinetic term.

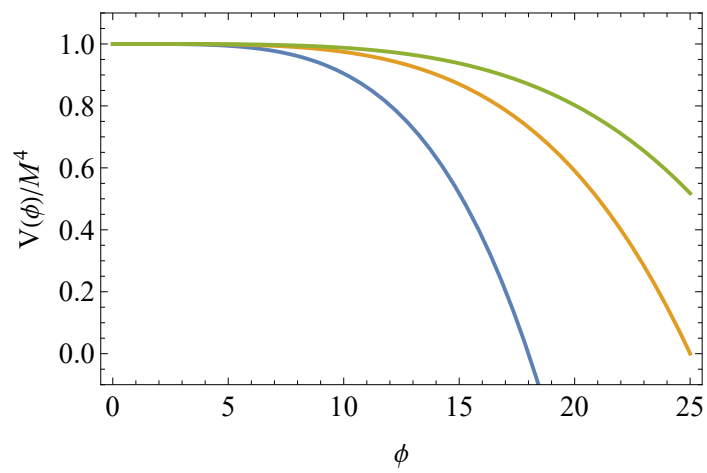


Figure 2.1: Hilltop potential for different values of the parameter μ : $\mu = 18$ (blue), $\mu = 25$ (orange), and $\mu = 30$ (green).

Chapter 3

Results & Discussion

Results obtained in this work will be separated in the following manner: first, the calculations for slow-roll parameters are outlined. These calculations yield essential values, such as the field quantities at the end and beginning of inflation, which are crucial for understanding the background dynamics. The outcomes of the slow-roll approximation and numerical results for the background dynamics are then presented in the following section. After that, there are shown perturbation analysis results and power spectra, along with the relationship of observable values like the spectral index and tensor-scalar ratio. Again these results were obtained for slow-roll approximation and for numerical results. Also, we note that all of this calculations were computed using a conventional laptop with AMD RYZEN 7 4000 series, using software Mathematica 13.3⁴¹, where the development of calculation have taken several hours, considering the range of parameters selected.

3.1 Slow-Roll Parameters

For Hilltop potential, the calculation of this quantities can be done analytically.

$$\epsilon = \frac{1}{2} \left[\frac{V'(\phi)}{V(\phi)} \right]^2, \quad (3.1)$$

$$= \frac{2p^2 \left(\frac{\phi}{\mu}\right)^{2p}}{\phi^2 \left[\left(\frac{\phi}{\mu}\right)^p - 1\right]^2}. \quad (3.2)$$

Considering that it is taken $p = 4$, because that is the model most favored by Plank's results¹, we obtained:

$$\epsilon = \frac{8\phi^6}{\mu^8 \left(1 - \frac{\phi^4}{\mu^4}\right)^2}. \quad (3.3)$$

This relation is shown in Fig. 3.1 for different values of μ .

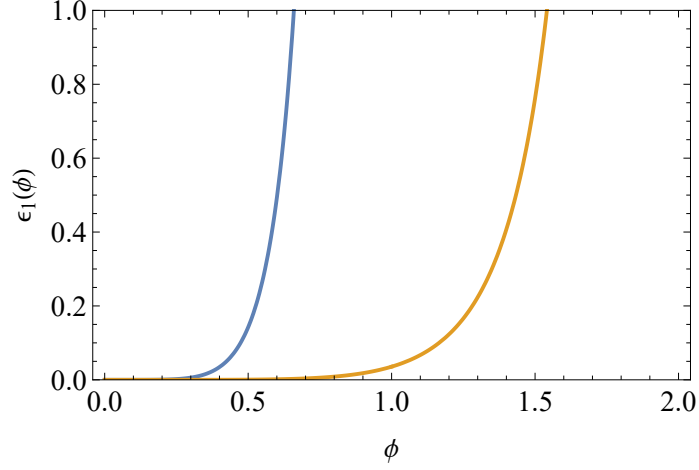


Figure 3.1: First slow roll parameter against the value of ϕ , for values of $\mu = 1$ (blue) and $\mu = 2$ (orange).

Now for obtaining the value ϕ_{end} , we equal $\epsilon = 1$, that is the conditions described in section 2 for the end of inflation.

$$\frac{8\phi_{\text{end}}^6}{\mu^8 \left(1 - \frac{\phi_{\text{end}}^4}{\mu^4}\right)^2} = 1. \quad (3.4)$$

Solving for ϕ_{end} , several solutions are obtained considering that we are dealing with a high-degree equation. However, considering the conditions of the Hilltop model, real and positive solutions are chosen. Additionally, this value has to be lower than the value selected for the parameter μ . According to¹, the range of parameter μ for which this potential has plausible solutions according to observations done by Planck's 2018, is:

$$-2 < \log_{10} \left(\frac{\mu}{M_{\text{pl}}} \right) < 2. \quad (3.5)$$

As units used for this work consider the term of Planck's mass as $M_{\text{pl}} = 1$, is obtained the following range:

$$0.01 < \mu < 100. \quad (3.6)$$

In Fig. 3.2, is shown the relation between the value chosen for the parameter μ , and its correspond value of ϕ_{end} considering the condition for the end of the inflation. After this, for the calculation of the value of the field ϕ at the beginning of the inflation it is necessary to consider the definition of amount of inflation, discussed in section 2.

$$N = \int_{\phi}^{\phi_{\text{ini}}} \frac{V(\phi)}{V_{\phi}(\phi)} d\phi. \quad (3.7)$$

where ϕ_{ini} represents the value of ϕ at the beginning of the inflation, and $V_{\phi}(\phi)$ represents the derivative of the potential respect to the field ϕ . With this equation, we calculated the number of e-folding at given value of ϕ . In this work the interest is in relating the quantity with a value for ϕ_{ini} . Developing this relation, we obtain:

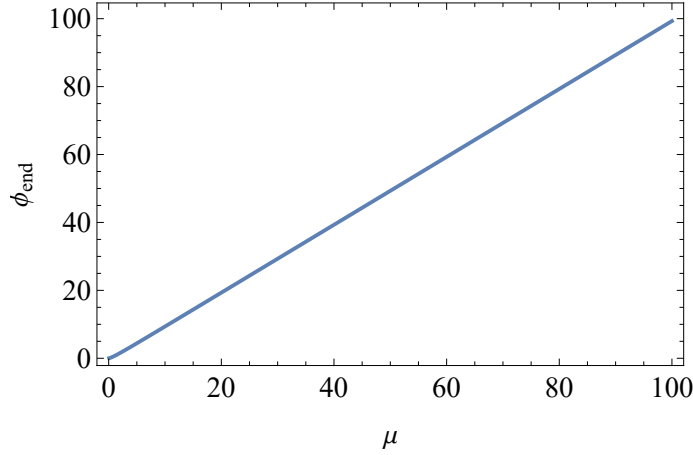


Figure 3.2: Relation between ϕ_{end} and μ , showing a linear pattern.

$$N = \frac{-\phi^2 + \phi_{\text{ini}}^2 - \frac{2\left[\phi^2\left(\frac{\phi}{\mu}\right)^{-p} - \phi_{\text{ini}}^2\left(\frac{\phi_{\text{ini}}}{\mu}\right)^{-p}\right]}{p-2}}{2p}, \quad (3.8)$$

$$N = \frac{1}{8} \left[\mu^4 \left(\frac{1}{\phi_{\text{ini}}^2} - \frac{1}{\phi^2} \right) + \phi_{\text{ini}}^2 - \phi^2 \right]. \quad (3.9)$$

Considering values for $N = 50$ and $N = 60$, according to the sections above, the conditions for the number of e-folding for the validity of Inflation theory, which is calculated $N \sim 55$. In that way, the following relations were obtained for each value, as shown in Fig. 3.3.

Having calculated values for the field ϕ at the end and at the beginning of inflation, now it is possible to use them to obtain solutions to the equations of motion of the universe. We will use these values to obtain solutions to slow-roll approximated equations, and then use them to calculate solutions for numerical approach. In the same way, during this process we will find the correct value for the M quantity, this value in the potential will help us as a normalization constant.

3.2 Slow Roll Background Solutions

For solving equations of motion of universe for the slow roll approximation:

$$H^2 \simeq \frac{1}{3}V(\phi), \quad (3.10)$$

$$3H\dot{\phi} \simeq -V_{\phi}. \quad (3.11)$$

Considering that $H = H(t)$ and $\phi = \phi(t)$, we get:

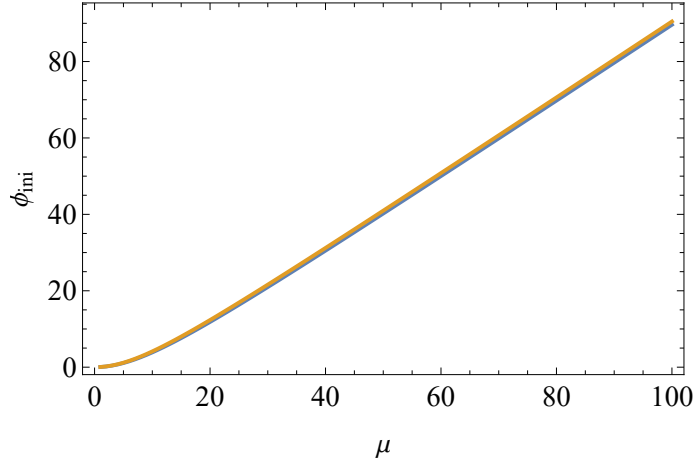


Figure 3.3: Relation between ϕ_{ini} and μ for $N = 60$ (blue), and $N = 50$ (orange).

$$H^2(t) \approx \frac{1}{3}V[\phi(t)], \quad (3.12)$$

$$3H(t)\dot{\phi}(t) \approx -\frac{\partial V[\phi(t)]}{\partial \phi(t)}, \quad (3.13)$$

$$\left[\frac{\dot{a}(t)}{a(t)}\right]^2 \approx \frac{1}{3}V[\phi(t)], \quad (3.14)$$

$$3\left[\frac{\dot{a}(t)}{a(t)}\right]\dot{\phi}(t) \approx -\frac{\partial V[\phi(t)]}{\partial \phi(t)}. \quad (3.15)$$

After this procedure, the value of ϕ_* is calculated. This value corresponds to the field at the horizon, and the condition used to calculate it is given by:

$$k = a(t)H(t), \quad (3.16)$$

where k represents the mode of oscillation, and for the purpose of this stage is taken $k = 0.05$.

Whit this is mind, there is developed a procedure in which is iteratively calculated ϕ_* until is obtained a convergence of this value. Then, having ϕ_* we used the equation that related the value of δ_R , reported by the Planck collaboration¹ in 2.1×10^{-9} , to compute:

$$\delta_R = \frac{1}{24\pi} \frac{V(\phi)}{\epsilon(\phi)}, \quad (3.17)$$

and after developing it:

$$M^4 = \frac{12\delta_R p^2 \pi^2 \left(\frac{\phi_*}{\mu}\right)^{2p}}{\phi_*^2 \left[1 - \left(\frac{\phi_*}{\mu}\right)\right]^3}. \quad (3.18)$$

Note that this relationship requires as one of its inputs the value of ϕ_* , the field at the horizon. This quantity M represents a free parameter that normalizes the scalar perturbation spectrum. In Figure 3.4, the relationship between this value and the parameter μ is illustrated.

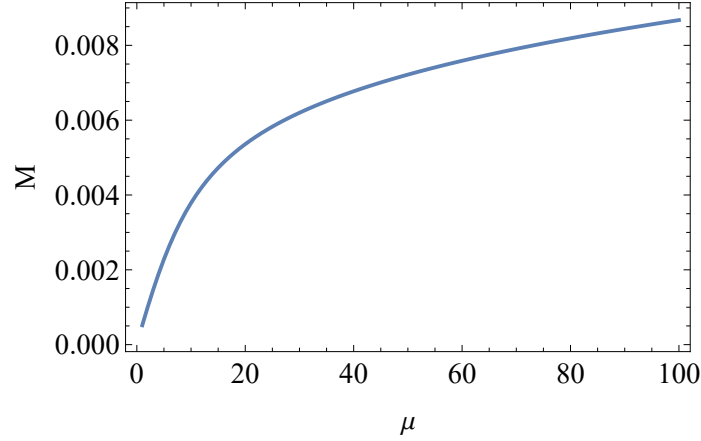


Figure 3.4: Relation between free parameter M and μ .

Having calculated this value, we can proceed to compute the solutions for the equations of motion, specifically for $\phi(t)$ and $a(t)$, which are presented in Figure 3.5. Fig. 3.5a illustrates the solution for scale factor $a_{sr}(t)$, showcasing its exponential shape. Additionally, Figure 3.5b displays the solution for the inflaton $\phi_{sr}(t)$, that goes from ϕ_{ini} to ϕ_{end} , that in this case for the parameter $\mu = 20$ are: $\phi_{ini} = 11.838$, and $\phi_{end} = 19.3287$.

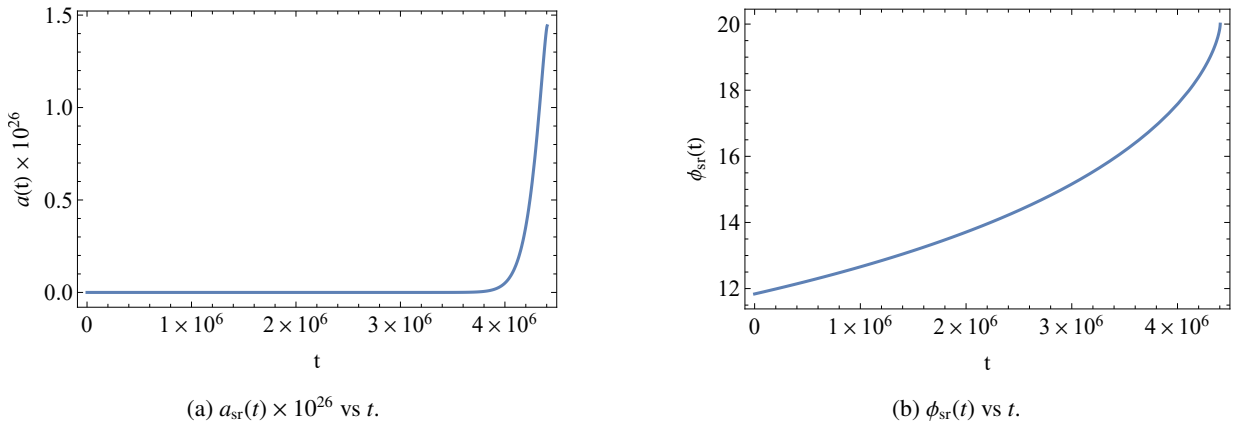


Figure 3.5: Plots of solutions of the background equations of motion under the slow-roll approximation, for scale factor a and inflaton field ϕ , for a fixed value of the parameter $\mu = 20$.

3.3 Slow Roll Perturbations

In previous chapter we have shown the development of the slow roll approximation and how this carry out to the expressions for the equations for observables, $P_S(k)$, $n_S(k)$ and $r(k)$.

$$P_S(k) = \frac{M^4}{144\pi^2 p^2} \left\{ -12\phi_*^2 \left[\left(\frac{\phi_*}{\mu} \right)^p - 1 \right]^2 + p \left(\frac{\phi_*}{\mu} \right)^p \left\{ 4 - 4p - 4 \left(\frac{\phi_*}{\mu} \right)^p + 5p \left(\frac{\phi_*}{\mu} \right)^p + 12C \left[\left(\frac{\phi_*}{\mu} \right)^p + p - 1 \right] \right\} \left(\frac{\phi_*}{\mu} \right)^{-2p} \left[\left(\frac{\phi_*}{\mu} \right)^p - 1 \right], \quad (3.19)$$

$$n_S(k) = 1 + p \left[2 - 2p - (2 + p) \left(\frac{\phi_*}{\mu} \right)^p \right] \frac{\left(\frac{\phi_*}{\mu} \right)^p}{\phi_*^2 \left[\left(\frac{\phi_*}{\mu} \right)^p - 1 \right]^2}, \quad (3.20)$$

$$r = 8p^2 \frac{\left(\frac{\phi_*}{\mu} \right)^{2p}}{\phi_*^2 \left[\left(\frac{\phi_*}{\mu} \right)^p - 1 \right]^2}, \quad (3.21)$$

where ϕ_* is the value of the inflaton field at the horizon.

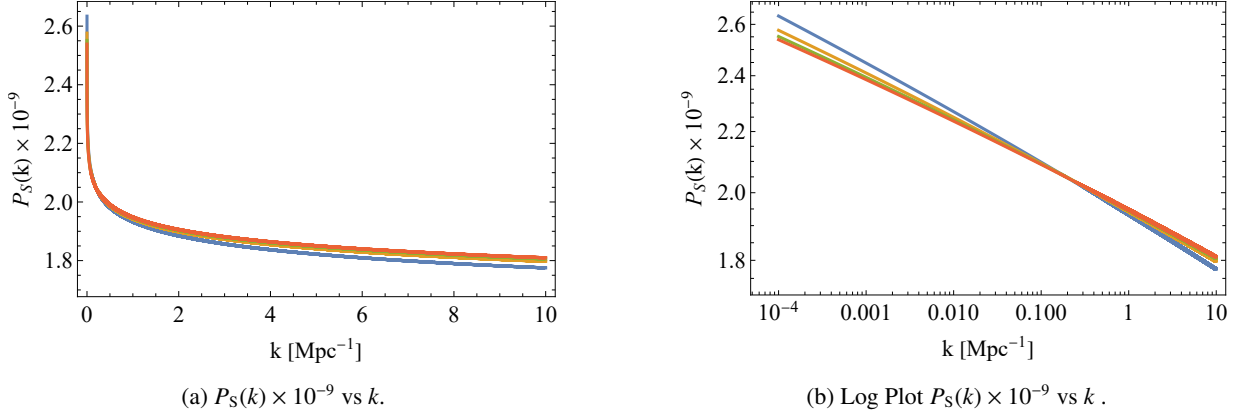


Figure 3.6: Plots of Scalar perturbation spectrum for different values of parameter μ : 20 (blue), 30 (orange), 40 (green), and 50 (red), into the slow roll approximation for $N = 60$.

In Fig. 3.5 we show solutions under the slow roll approximation, illustrating the scalar perturbation spectrum for different values of parameter μ , there are presented in normal scale and in log scale. This last provides a clearer depiction of the differences between each of the cases, highlighting how the slope of the curve changes as it is changed parameters of model.

Observables of the model are seen in Fig. 3.7, we present the relation of spectral index, tensor scalar ratio and the parameter μ at the pivot scale $k = 0.002 \text{ Mpc}^{-1}$, and for values $N = 50$ and $N = 60$ into the slow roll approximation.

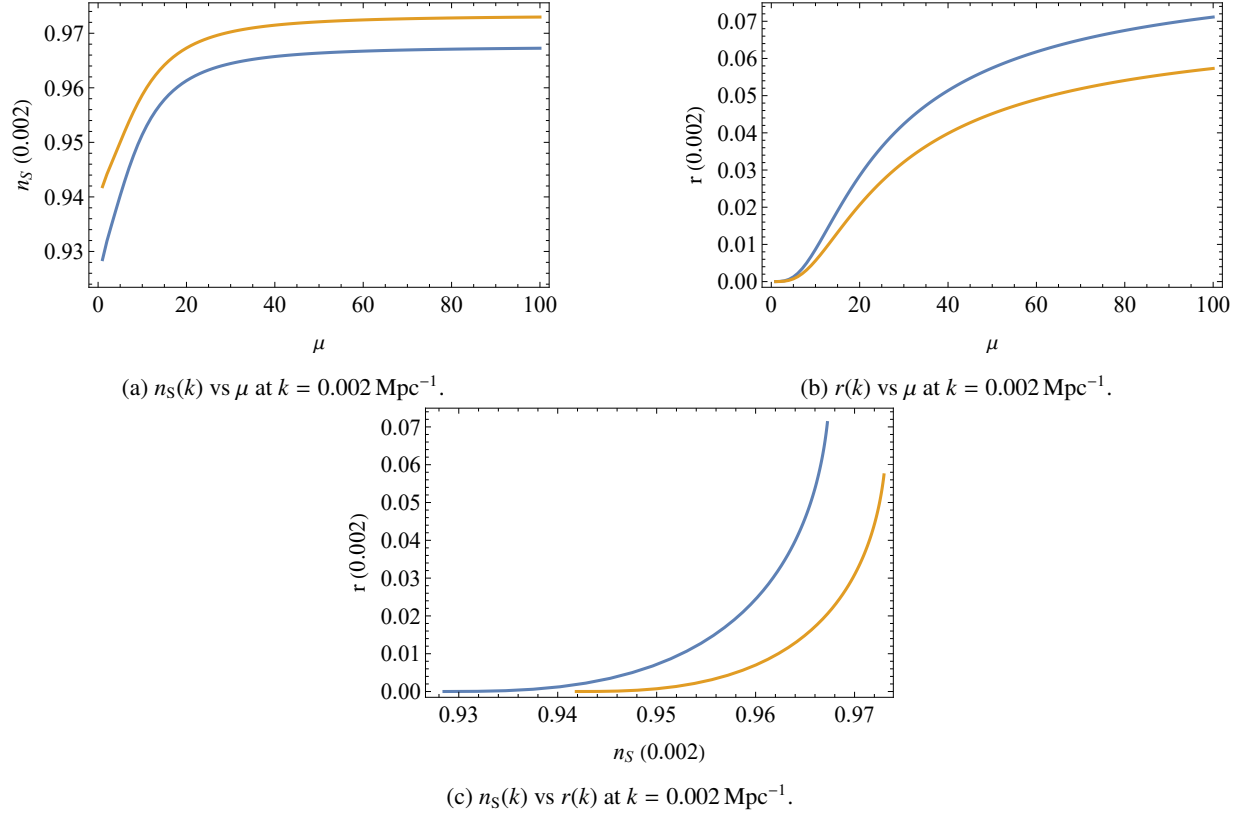


Figure 3.7: Plots of relation of observable against the parameter μ for $N = 50$ (blue) and $N = 60$ (orange) for slow roll approximation. a) profile of spectral index $n_s(k)$ evaluated at $k = 0.002 \text{ Mpc}^{-1}$ against μ , b) profile of tensor scalar ratio $r(k)$ evaluated at $k = 0.002$ against μ and c) profile of spectral index $n_s(k)$ evaluated at $k = 0.002 \text{ Mpc}^{-1}$ against tensor scalar ratio $r(k)$ evaluated at $k = 0.002 \text{ Mpc}^{-1}$

3.4 Numerical Background Solutions

For numerical resolution of background solutions we used complete equations of motion of the universe:

$$H^2 = \frac{1}{3} \left[V(\phi) + \frac{1}{2} \dot{\phi}^2 \right], \quad (3.22)$$

$$\ddot{\phi} + 3H\dot{\phi} = -V_\phi(\phi). \quad (3.23)$$

We used Mathematica function *NDSolve* to obtain a numerical result for each of the functions, the inflation field $\phi(t)$ and $a(t)$. And as initial conditions are used the result obtained from slow roll approximation in the last section evaluated at $t = 0$.

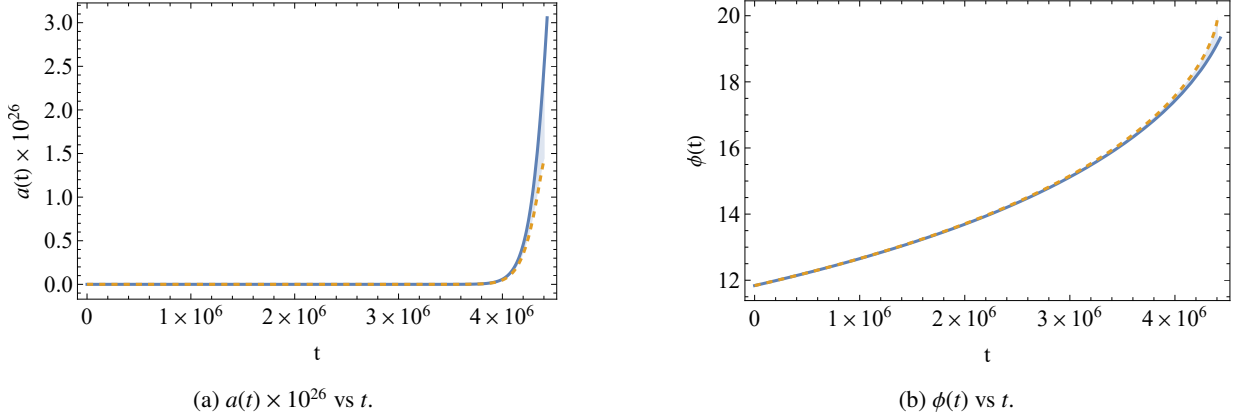


Figure 3.8: Plots of numerical solutions (solid) and slow roll (dashed) of the background equations of motion, for scale factor a and inflaton field ϕ , for a fixed value of the parameter $\mu = 20$.

In Fig. 3.8a we show the evolution of the scale factor a over cosmic time t , and in Fig. 3.8b we show the evolution of the inflation field ϕ over cosmic time t , for number of e-folding $N = 60$ and parameter $\mu = 20$. Also in both figures in Fig. 3.8 it is compared numerical result and the result obtained from slow roll approximation, showing that for most of the time the approximation works well, and the difference between them is small. However, for values of time close to the end of the inflation, slow roll and numerical results start to separate, this difference can be seen also in the calculated value for the t_{end} , the time at the end of inflation, as it can be seen in tab. 3.1.

N	μ	Slow roll	Numerical
50	20	3.07717×10^6	3.13727×10^6
60	20	4.35531×10^6	4.43099×10^6

Table 3.1: Values of t_{end} for parameter selection $\mu = 20$, for $N = 60$ and $N = 50$.

3.5 Numerical Perturbation Solutions

Numerical calculation of perturbations involve solving the Mukhanov-Sasaki equation for the variable v_k , considering it in cosmic time t form, when t is taken as independent variable. The relation between conformal η and cosmic time t is given by the expression:

$$dt = ad\eta. \quad (3.24)$$

Fig. 3.9 shows this relation, solving for imposed condition $\eta(t_{\text{end}}) = 0$. In that way we pass from perturbation equations with derivatives with respect to conformal time:

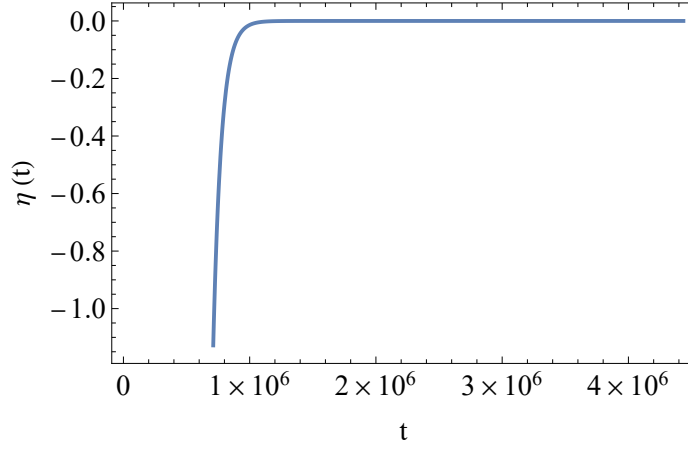


Figure 3.9: Relation of conformal η and cosmic time t for $\mu = 20$ and $N = 60$.

$$u_k'' + \left(k^2 - \frac{z_s''}{z_s} \right) u_k = 0, \quad (3.25)$$

$$v_k'' + \left(k^2 - \frac{a''}{a} \right) v_k = 0, \quad (3.26)$$

to equations with derivatives with respect to cosmic time:

$$\ddot{u}_k + \frac{\dot{a}}{a} \dot{u}_k + \frac{1}{a^2} \left[k^2 - \frac{(\dot{a}z_s + a\ddot{z}_s)a}{z_s} \right] u_k = 0, \quad (3.27)$$

$$\ddot{v}_k + \frac{\dot{a}}{a} \dot{v}_k + \frac{1}{a^2} \left[k^2 - (\dot{a}^2 + a\ddot{a}) \right] v_k = 0. \quad (3.28)$$

From Eq. 3.27 and Eq. 3.28, functions u_k and v_k are complex, then they have a real and an imaginary component, for that reason there are solved two differential equations for each of the expressions above. In the same way, these equations are solved in two parts: the first in which is considered the case when $k^2 \gg \frac{(\dot{a}z_s + a\ddot{z}_s)a}{z_s}$ and $k^2 \gg (\dot{a}^2 + a\ddot{a})$ in scalar and tensor perturbation equations respectively, this reduces equations to Eq. 3.29 and Eq. 3.30, and in second place are considered full equations. This parts corresponds to solutions inside and outside the horizon respectively.

$$\ddot{u}_k + \frac{\dot{a}}{a} \dot{u}_k + \frac{k^2}{a^2} u_k = 0, \quad (3.29)$$

$$\ddot{v}_k + \frac{\dot{a}}{a} \dot{v}_k + \frac{k^2}{a^2} v_k = 0. \quad (3.30)$$

In Fig. 3.10 we show the result of scalar perturbation differential equation, Eq 3.27, for different sets of parameters. Notice that Fig. 3.10a and Fig. 3.10c illustrate the solution of the real component of v_k function, and Fig. 3.10b and Fig. 3.10d the solution of the imaginary component. These figures show how change the v_k function when is changed the value of N : $N = 60$ and $N = 50$, and how they change after changing the value of μ : $\mu = 20$ and

$\mu = 30$. They show that the effect after changing the value of e-foldings N is small, it can be seen, but for example horizon crossing time is almost the same. But when it is seen the effect of changing parameter μ , this change is more noticeable, in the shape and localization of the function, and in the location of the horizon crossing time, for both real and imaginary components.

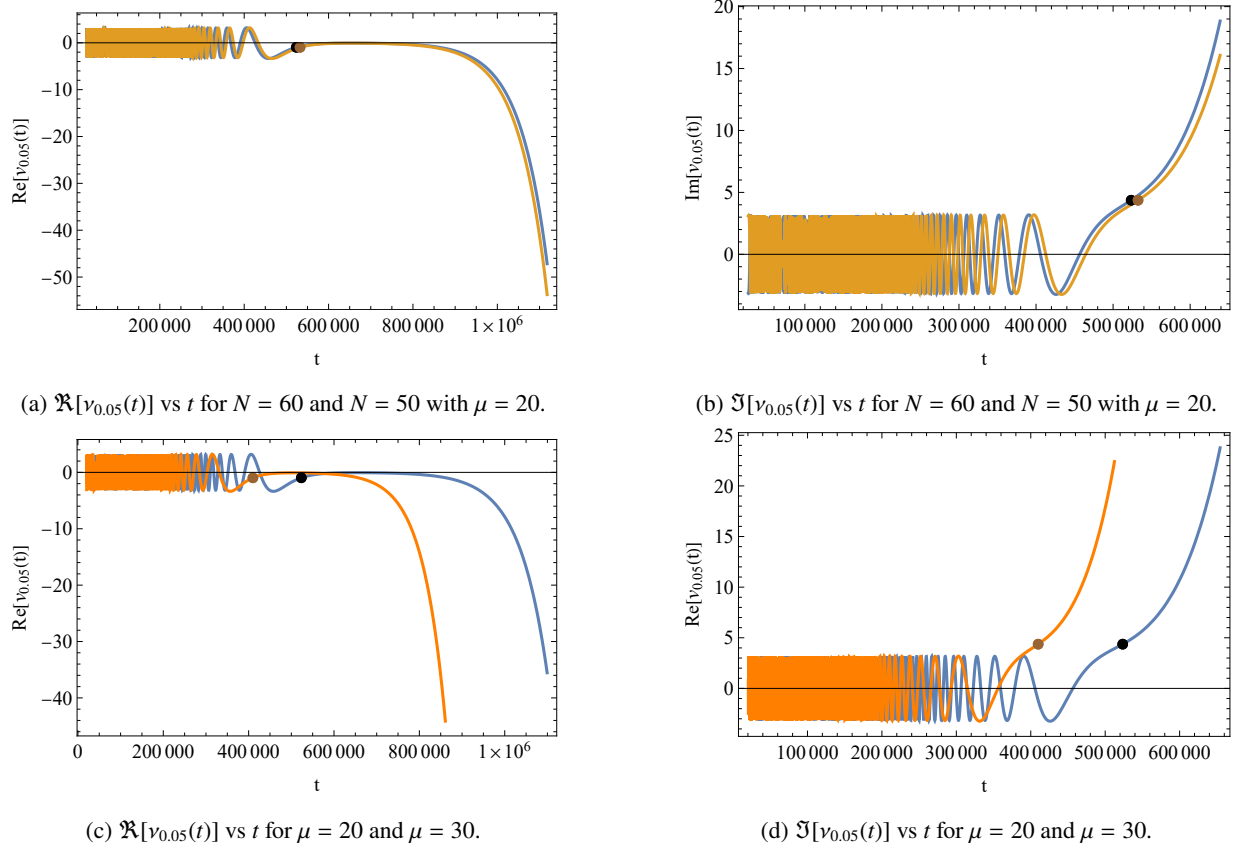


Figure 3.10: Plots of the components of ν_k evaluated at pivot scale $k = 0.05 \text{ Mpc}^{-1}$ for different parameters of the model a) and b) represents real and complex components comparing between $N = 60$ (blue) and $N = 50$ (orange) and with black and brown points representing the point of horizon crossing in each respective case, both with a fixed parameter $\mu = 20$. c) and d) represents real and complex components comparing between two different values of μ : $\mu = 20$ (blue) and $\mu = 30$ (orange). Black and brown points represent the horizon crossing in each case .

After obtaining these solutions we used Eq. 2.49 and Eq. 2.50, that relate the result functions of differential equations above, to obtain scalar and tensor perturbation spectrum for given pivot scale k_* . There are obtained values for P_S and P_T , for values of k_* from 0.001 to 2.5. The data is then used to fit and obtain the function based on the shapes defined in Equations 2.54 and 2.55. This process yields coefficients, namely, the scalar spectral index n_S and the running index value α .

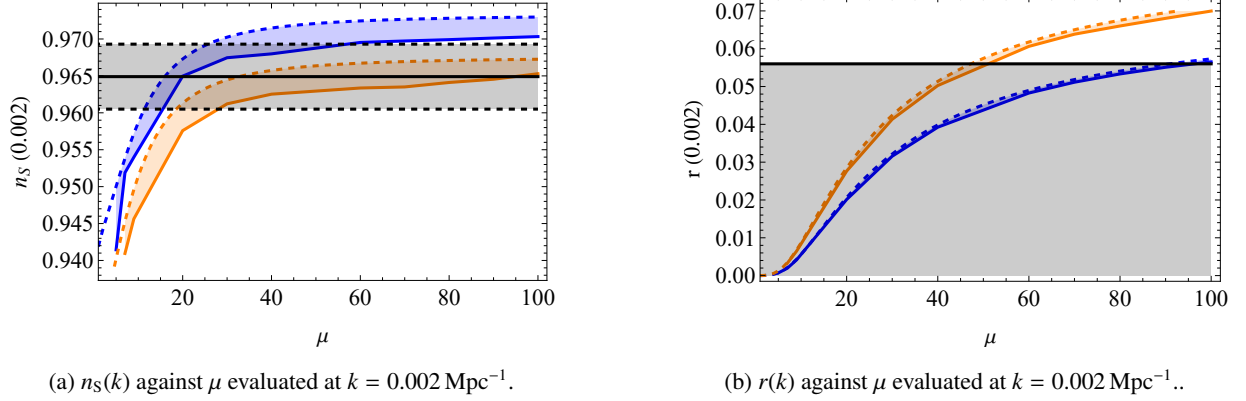


Figure 3.11: Comparison of numerical (solid curves) and slow roll (dashed curves) results of $n_s(k)$ and $r(k)$ evaluated at $k = 0.002 \text{ Mpc}^{-1}$, compared for different values of μ , considering $N = 60$ (blue) and $N = 50$ (orange), also it is shown values of observational results obtained by Planks 2018¹ ($n_s = 0.9649 \pm 0.0042$ and $r < 0.056$).

These results are presented in Fig. 3.11, each subplot show the behavior of spectral index $n_s(k)$ evaluated at $k = 0.002 \text{ Mpc}^{-1}$ and the tensor scalar ratio $r(k)$ evaluated at the same pivot scale. In plots we have shown how these values change with the variation of the parameter μ , in the case of n_s against μ plot, Fig. 3.11a, the value of n_s increases as the value of μ is incremented. This behavior is maintained for numerical and slow roll results, and also the same behavior appears for $N = 60$ and $N = 50$. In the other side, the plot of the resulted values of r , the behavior of slow roll and numerical approach are quite similar. Also it is noticed that for very small values of μ the values of r get close for $N = 60$ and $N = 50$, reducing their difference.

Also, these results are compared with observational values. Fig. 3.11 shows a black region that represents these quantities. It is observed that this area have overlapping regions with results obtained in this work. In the case of n_s values for which there is an agreement depends on the selected value of N . For the case of $N = 60$, there exist to ranges of parameter μ for which is fulfil these condition: the first one that represent the observable obtained from slow roll calculations (dashed curves) and the second one that is obtained from numerical approach (solid curves). For the first condition the values are approximately $12 < \mu < 26$ and for the second condition $16 < \mu < 56$. It is noticed that there exist a window for which both approaches converge. In the case of $N = 50$, the range for slow roll result is $\mu > 19$ and for numerical $\mu > 28$.

In the case of r , the ranges of parameter μ that agree with the result of Planks 2018 are: in the case of $N = 60$, $\mu < 90$ for slow roll, and $\mu < 96$ for numerical approach. For $N = 50$ the ranges are: $\mu < 47$ for slow roll, and $\mu < 52$ for numerical result.

Then, it can be obtain the relation between these observables, which is shown in Fig. 3.12. This plot relates the values of scalar spectral index $n_s(k)$ and the tensor scalar ratio $r(k)$, both evaluated at a pivot scale $k = 0.002 \text{ Mpc}^{-1}$.

Finally, we presented the scalar perturbation spectrum for a selection of values of μ . Fig. 3.13 shows the relation of this spectrum with k , in normal scale, Fig. 3.13a, and in log scale, Fig. 3.13b. In the first one can be noticed the

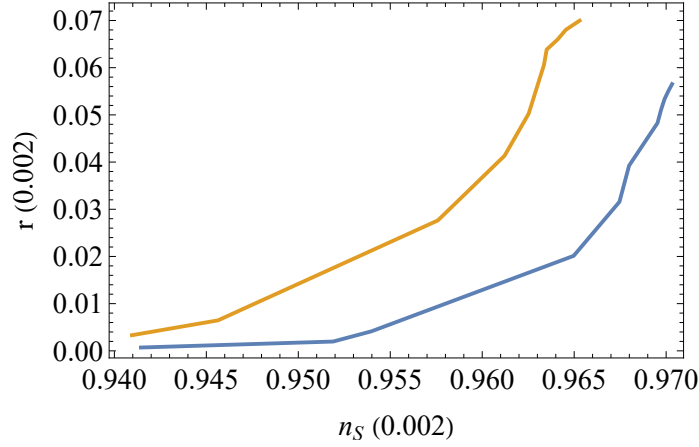


Figure 3.12: Relation between numerical calculation of $n_s(k)$ vs $r(k)$ evaluated at $k = 0.002 \text{ Mpc}^{-1}$ for different values of μ considering $N = 50$ (orange) and $N = 60$ (blue).

difference between $\mu = 20$ and the other cases, but these last do not differ so much between them. Log plot allows to distinct between them, showing different slopes for the curve, for each value of μ . It is observed that for small values of k exist a linear relation in the log plot between $P_S(k)$ and k , but this linear regression is not maintain because the dispersion of curves is changed for greater values of k .

In the last plot, Fig. 3.13c shows the comparison between numerical and slow roll results for scalar perturbations spectrum, in this case it is taken $\mu = 20$ and $\mu = 30$. We observed that there is a strong correspondence between the results obtained from these approaches for small values of k . However, as the value of k increases, the calculations begin to diverge. This discrepancy becomes significant for values of k between 5 and 10.

Finally it has been found that exist a range of parameter μ for which there is a great agreement between observational parameters with observational results from Planck collaboration. This range depends on the number of inflation, N , with which the work is done. But there are some region of the space of possible parameters that is valid for both branches of the work, for $N = 50$ and for $N = 60$. For the scalar spectral index, n_s , this range is between $19 > \mu > 26$ for slow roll and $28 > \mu > 56$ for numerical approach. And for tensor scalar ratio the range is $\mu < 47$ for slow roll and $\mu < 52$ in the numerical case. This results shows that this model can be taken as an important candidate for inflation considering that results on slow roll approach and numerical outcome are highly favoured by Planck 2018 data release¹.

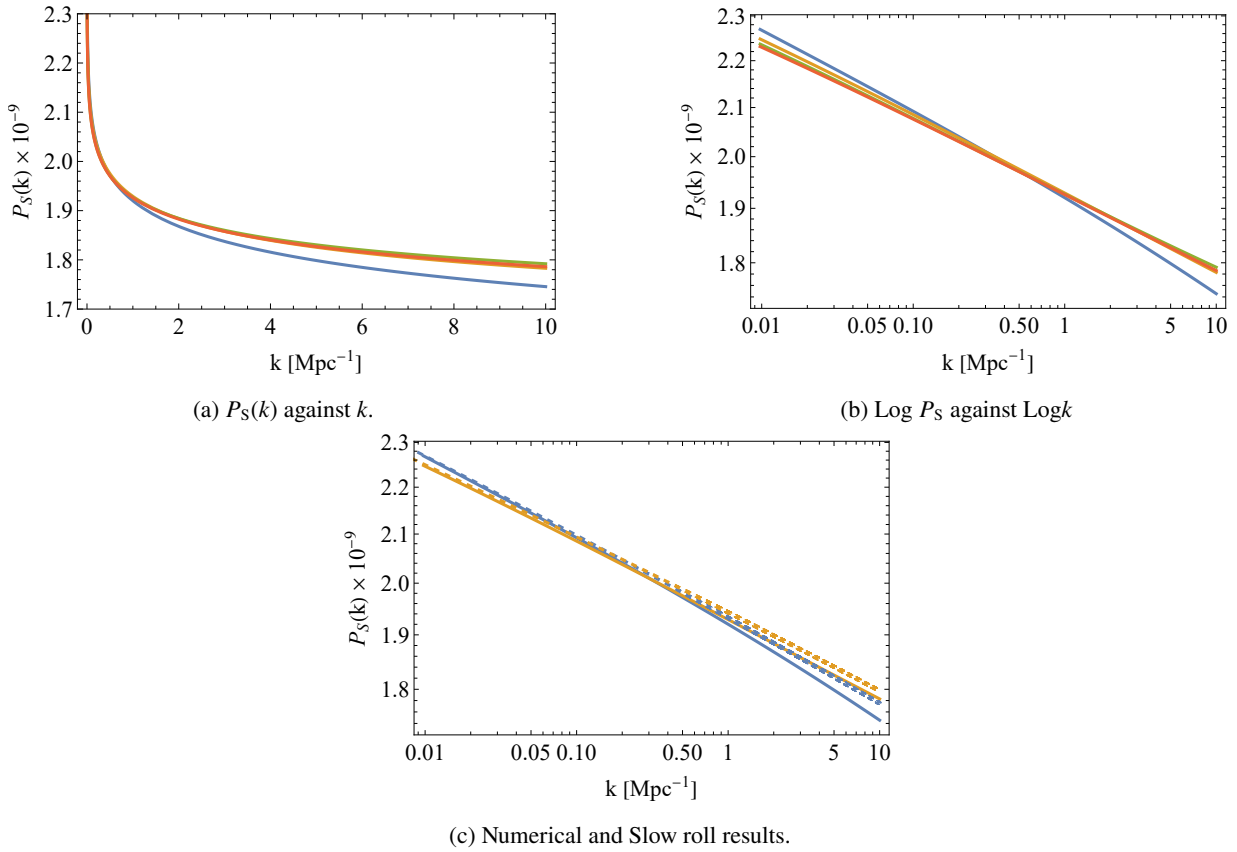


Figure 3.13: a) Scalar perturbations spectrum from numerical approach against k , b) Log plot of scalar perturbation spectrum, both for $\mu = 20$ (blue), $\mu = 30$ (orange), $\mu = 40$ (green), and $\mu = 50$ (red).c) Comparison between slow roll (dashed) and numerical (solid) result of $P_S(k)$ for $\mu = 20$ (blue) and $\mu = 30$ (orange).

Chapter 4

Conclusions & Outlook

In this work it is reviewed some of the fundamental concepts necessary to go further in the topic of inflationary cosmology, there is introduced the theory behind the Hot Big Bang Model and some of the puzzles created by this approach. Also the main equations used in cosmology are developed and explained. Then it is presented inflation as a solution of this puzzles and more problems that at the moment of the development of the theory were still a mystery, like the way early universe and large scale structure were related or the discrepancies in the distribution of temperatures in the CMB.

There is introduced also the motivation and application of the slow-roll approximation used to understand inflationary models under the assumption of dominance of potential over the kinetic term in the equations of motion of the universe. There are defined some of the most important parameters for this analysis. There is also a section about cosmological perturbation theory where is explained and defined some of the gauge invariant variables necessary to obtain information about the cosmological observables of the universe, that are useful to connect the work done theoretically and computationally with the work done by observations. In the same chapter is introduced the potential that is used for this work, the hilltop potential.

The chapter corresponding to the results contains all the information about the analysis that was conducted, in both of the approaches used: slow-roll approximation and numerical results. This chapter is also divided in background and perturbations results. Using calculations done with slow-roll parameters, and the definition of the amount of inflation, there are computed features like the value of the field at the beginning and at the end of the inflation. There are presented the solutions for the equations of motion of the universe giving plots that relate the evolution of the inflaton field $\phi(t)$ and the scale factor $a(t)$.

Using differential equations governing the evolution of the scalar and tensor perturbations there are calculated the functions that relate the behavior in time of the gauge invariant variables defined u_k and v_k that related the modes of the perturbations. With definitions provided in Chapter. 2 about scalar and tensor power spectrum, there is obtained information for different values of scale k necessary to find the best fit according to the definition of these spectra as power law.

Finally, there are obtained values of the observables: spectral index $n_S(k)$ and tensor-scalar ratio $r(k)$ evaluated

at $k = 0.002 \text{ Mpc}^{-1}$ for different values of the parameter μ in the range. This calculation is performed using both the slow-roll approximation and numerical approach, then is make a comparison between these methods and its results. Furthermore these results is compared with the values reported by the Plank's experiment. In conclusion, the Hilltop quartic model appears to be favored by the observational results, and a confident range of parameters can be chosen based on this concordance. For numerical case the range of parameter μ that agrees with Plank's result is $16 < \mu < 56$ if it is used as discriminator the value of n_s considering the number of e-foldings $N = 60$. And using tensor-scalar ratio r the range is $\mu < 90$. It can be seen that there is an intersection between these ranges $16 < \mu < 56$.

For the case $N = 50$, when using n_s as the discriminator, the obtained range is $\mu > 28$, and using r is $\mu < 52$. The intersection of these sets is: $28 < \mu < 52$. After this it is obtained plots about scalar power spectrum.

The constraint of inflationary models heavily relies on the results obtained from observational efforts. Advancements in this field, particularly improvements in the accuracy of observable measurements, directly impact its development. Future work in this area must take this fact into account, and also consider different observational results that until now has carried us to the "CMB tension".

Appendix A

Mathematica Code Used

Listing A.1: Code for obtaining values for ϕ_{end} , ϕ_{ini} and M given μ , p and a value for ϕ_* .

```
1 cend = Compile[{{p, _Real}, {\[Mu], _Real}},
2   end\[Phi] =
3     SolveValues[(p^2 (\[Phi]/\[Mu])^(-2 + 2 p))/(
4       2 \[Mu]^2 (1 - (\[Phi]/\[Mu])^p)^2) == 1, \[Phi],
5     Assumptions -> {\[Phi] > 0, \[Phi] < \[Mu]}] // N];
6 cini = Compile[{{p, _Real}, {\[Mu], _Real}},
7   end\[Phi] = cend[p, \[Mu]];
8   ini\[Phi] =
9     SolveValues[(-\[Phi]^2 + \[Phi]i^2 - (
10       2 (\[Phi]^2 (\[Phi]/\[Mu])^-p - \[Phi]i^2 \
11 (\[Phi]i/\[Mu])^-p))/(-2 + p))/(2 p) - 60 == 0 /. \[Phi] ->
12     end\[Phi], \[Phi]i,
13     Assumptions -> {\[Phi]i > 0, \[Phi]i < \[Mu]}] // N ];
14
15 cM = Compile[{{p, _Real}, {\[Mu], _Real}, {\[Phi]p, _Real}},
16   end\[Phi] = cend[p, \[Mu]];
17   ini\[Phi] = cini[p, \[Mu]];
18   deltaR = 2.1 10^-9;
19   M = (-((
20     12 deltaR p^2 \[Pi]^2 (\[Phi]p/\[Mu])^(
21     2 p))/(\[Phi]p^2 (-1 + (\[Phi]p/\[Mu])^p)^3)))^(1/4)];
```

Listing A.2: Code for calculation of ϕ_* and M under the slow roll approximation for a given value of μ .

```

1 c\[Phi]evalsr =
2 Compile[{{p, _Real}, {\[Mu], _Real}, {\[Phi]p, _Real}},
3   \[Phi]ini = cini[p, \[Mu]];
4   M = cM[p, \[Mu], \[Phi]p];
5   V[p, t] = M^4 (1 - (\[Phi]s[t]/\[Mu])^p);
6   Vp[p, t] = D[V[p, t], \[Phi]s[t]];
7   sol =
8     NDSolve[{\[Phi]s'[t] == - Vp[p, t] as[t]/(3 as'[t]) ,
9     as'[t] ==
10     as[t] Sqrt[1/3 V[p, t]], \[Phi]s[0] == \[Phi]ini[[1]],
11     as[0] == 1}, {\[Phi]s, as}, {t, 0, 4.06 10^8}];
12   asr[t_] = (as /. First[sol])[t];
13   asrp[t_] = D[asr[t], {t, 1}];
14   \[Phi]sr[t_] = (\[Phi]s /. First[sol])[t];
15   \[Phi]srp[t_] = D[\[Phi]sr[t], {t, 1}];
16   H[t_] = pa[t]/a[t];
17
18   teval[k_] = FindRoot[k == asrp[t], {t, 10^7}];
19   \[Phi]sr[teval[0.05][[1, 2]]];
20
21 p = 4;
22 \[Mu] = 1;
23 \[Phi]eval[\[Phi]h_] := c\[Phi]evalsr[p, \[Mu], \[Phi]h]
24
25 attemp = cini[p, \[Mu]];
26 iterations = 10;
27 his = NestList[\[Phi]eval, attemp, iterations]
28
29 Mvalue[\[Phi]h_] := cM[p, \[Mu], \[Phi]h]
30 Mvalue[his[[-1]]]

```

Listing A.3: Code for calculation of ϕ_* and M for a given value of μ .

```

1 c\[Phi]eval =
2 Compile[{{p, _Real}, {\[Mu], _Real}, {\[Phi]p, _Real}},
3   \[Phi]ini = cini[p, \[Mu]];
4   M = cM[p, \[Mu], \[Phi]p];
5   V[p, t] = M^4 (1 - (\[Phi]s[t]/\[Mu])^p);

```



```

6 Vp[p, t] = D[V[p, t], \[Phi]s[t]];
7 sol = NDSolve[{\[Phi]s'[t] == - Vp[p, t] as[t]/(3 as'[t]) ,
8   as'[t] == as[t] Sqrt[1/3 V[p, t]], \[Phi]s[0] == \[Phi]ini[[1]],
9   as[0] == 1}, {\[Phi]s, as}, {t, 0, 4.06 10^8}];
10 asr[t_] = (as /. First[sol])[t];
11 asrp[t_] = D[asr[t], {t, 1}];
12 \[Phi]sr[t_] = (\[Phi]s /. First[sol])[t];
13 \[Phi]srp[t_] = D[\[Phi]sr[t], {t, 1}];
14 Vt[t_] = M^4 (1 - (\[Phi]t[t] / \[Mu])^p);
15 Vtp[t_] = D[Vt[t], \[Phi]t[t]];
16 sol1 =
17 NDSolve[{\[Phi]t''[t] + 3 at'[t]/at[t] \[Phi]t'[t] + Vtp[t] == 0,
18   at'[t] == at[t] Sqrt[1/3 (1/2 \[Phi]t'[t]^2 + Vt[t])], \[Phi]t[
19   0] == \[Phi]sr[0], \[Phi]t'[0] == \[Phi]srp[0],
20   at[0] == 1}, {\[Phi]t, at}, {t, 0, 4.06 10^8}];
21 \[Phi][t_] = (\[Phi]t /. First[sol1])[t];
22 a[t_] = (at /. First[sol1])[t];
23 pa[t_] = (at' /. First[sol1])[t];
24 H[t_] = pa[t]/a[t];
25
26 teval[k_] = FindRoot[k == pa[t], {t, 10^8}];
27 Print[teval[0.05]];
28 \[Phi][teval[0.05][[1, 2]]];
29
30 p = 4;
31 \[Mu] = 1;
32 \[Phi]eval\[Phi]h_ := c\[Phi]evalsr[p, \[Mu], \[Phi]h]
33
34 attemp = cini[p, \[Mu]];
35 iterations = 10;
36 his = NestList[\[Phi]eval, attemp, iterations]
37
38 Mvalue\[Phi]h_ := cM[p, \[Mu], \[Phi]h]
39 Mvalue[his[[-1]]]

```

Listing A.4: Code for calculation of background solutions of $\phi(t)$ and $a(t)$ under slow roll approximation.

```

1 \[Mu] := 20
2 M := 0.005359077192041455 '

```

```

3 p := 4
4 \[Phi]ini = 11.838012784632001';
5 \[Phi]end = 19.328683873439395';
6 V[p_, t_] := M^4 (1 - (\[Phi][t]/\[Mu])^p)
7 Vp[p_, t_] = D[V[p, t], \[Phi][t]];
8 ten = 4.57 10^6;
9 sol = NDSolve[{ 3 a'[t]/a[t] \[Phi]'[t] + Vp[p, t] == 0,
10   a'[t] == a[t] Sqrt[1/3 (V[p, t])],
11   \[Phi][0] == \[Phi]ini, a[0] == 1}, {\[Phi], a},
12   {t, 0, ten}, MaxSteps -> 10000000, AccuracyGoal -> 10];
13 \[Phi]sr1[t_] := (\[Phi] /. First[sol])[t]
14 \[Phi]srp[t_] = D[\[Phi]sr1[t], {t, 1}];
15 asr[t_] := (a /. First[sol])[t]
16 tend = t /. FindRoot[\[Phi]sr1[t] == \[Phi]end, {t, ten }];

```

Listing A.5: Code for calculation of background solutions of $\phi(t)$ and $a(t)$ numerically.

```

1 \[Mu] := 20
2 M := Import[
3   "C:\\Users\\RAUL\\Documents\\Wolfram_Mathematica\\Titulation_-\[
4   Cosmology\\data_ex\\mvalues_ex_k005_N60.csv"][[\[Mu], 2]];
5 p := 4
6 \[Phi]end := First[cend[p, \[Mu]]]
7 \[Phi]ini := First[cini[p, \[Mu]]]
8 V[t_] := M^4 (1 - (\[Phi][t]/\[Mu])^p)
9 Vp[t_] = D[V[t], \[Phi][t]];
10 ten := 4.57 10^6
11 (*\[Phi]sr, asr*)
12 sol = NDSolve[{ 3 a'[t]/a[t] \[Phi]'[t] + Vp[t] == 0,
13   a'[t] == a[t] Sqrt[1/3 (V[t])],
14   \[Phi][0] == \[Phi]ini, a[0] == 1}, {\[Phi], a},
15   {t, -90000, ten}, MaxSteps -> 100000, AccuracyGoal -> 10];
16 \[Phi]sr[t_] := (\[Phi] /. First[sol])[t]
17 \[Phi]srp[t_] = D[\[Phi]sr[t], {t, 1}];
18 asr[t_] := (a /. First[sol])[t];
19 (*\[Phi], a*)
20 Vt[t_] := M^4 (1 - (\[Phi]t[t]/\[Mu])^p)
21 Vtp[t_] = D[Vt[t], \[Phi]t[t]];
22 sol1 = NDSolve[{\[Phi]t'[t] + 3 at'[t]/at[t] \[Phi]t'[t] + Vtp[t] ==

```

```

23     0,
24     at'[t] == at[t] Sqrt[1/3 (1/2 \[Phi]t'[t]^2 + Vt[t])],
25     \[Phi]t[0] == \[Phi]sr[0], \[Phi]t'[0] == \[Phi]srp[0],
26     at[0] == 1}, {\[Phi]t, at},
27     {t, -90000, ten}, MaxSteps -> 100000, AccuracyGoal -> 10];
28 \[Phi][t_] := (\[Phi]t /. First[sol1])[t]
29 p\[Phi][t_] := (\[Phi]t' /. First[sol1])[t];
30 pp\[Phi][t_] := (\[Phi]t'' /. First[sol1])[t];
31 ppp\[Phi][t_] := (\[Phi]t''' /. First[sol1])[t];
32 a[t_] := (at /. First[sol1])[t];
33 pa[t_] := (at' /. First[sol1])[t];
34 ppa[t_] := (at'' /. First[sol1])[t];
35 pppa[t_] := (at''' /. First[sol1])[t];

```

Listing A.6: Code for calculation of perturbations and observables under slow roll calculations.

```

1  M := 0.005131259185052941'
2  p := 4
3  \[Mu] := 18
4  \[Phi]ini = 10.106728678999152';
5  \[Phi]end = 17.332457543904017';
6  V[p_, t_] := M^4 (1 - (\[Phi][t]/\[Mu])^p)
7  Vp[p_, t_] = D[V[p, t], \[Phi][t]];
8  sol = NDSolve[{\[Phi]'[t] == - Vp[p, t] a[t]/(3 a'[t]) ,
9     a'[t] == a[t] Sqrt[1/3 V[p, t]], \[Phi][0] == \[Phi]ini,
10    a[0] == 1}, {\[Phi], a}, {t, 0, 9 10^6}];
11 asr[t_] := (a /. First[sol])[t]
12 asrp[t_] = D[asr[t], {t, 1}];
13 \[Phi]sr[t_] := (\[Phi] /. First[sol])[t]
14 \[Phi]srp[t_] = D[\[Phi]sr[t], {t, 1}];
15 \[Phi]srpp[t_] = D[\[Phi]sr[t], {t, 2}];
16 \[Phi]srppp[t_] = D[\[Phi]sr[t], {t, 3}];
17 Vt[p_, t_] := M^4 (1 - (\[Phi]sr[t]/\[Mu])^p)
18 Hsr[p_, t_] := 1/Sqrt[3] Sqrt[Vt[p, t]]
19 Hsrp[p_, t_] = D[Hsr[p, t], {t, 1}];
20 Vphi[p_, \[Phi]_] := M^4 (1 - (\[Phi]/\[Mu])^p)
21 Vphip[p_, \[Phi]_] := D[Vphi[p, \[Phi]], {\[Phi], 1}];
22 Vphipp[p_, \[Phi]_] := D[Vphi[p, \[Phi]], {\[Phi], 2}];
23 (*Parameters*)

```

```

24 \[Epsilon]H1[p_, t_] := -Hsrp[p, t]/Hsr[p, t]^2
25 \[Epsilon]H2[p_, t_] = 1/Hsr[p, t] D\[Epsilon]H1[p, t], {t, 1}];
26 \[Delta]H1[p_, t_] := \[Phi]srpp[t]/(Hsr[p, t] \[Phi]srp[t])
27 \[Delta]H2[p_, t_] := \[Phi]srppp[t]/(Hsr[p, t]^2 \[Phi]srp[t])
28 \[Alpha] := 0.729637
29 (*First Order*)
30 PSsr1[t_] := (1 + (4 \[Alpha] - 2) \[Epsilon]H1[p, t] +
31     2 \[Alpha] \[Delta]H1[p, t]) (Hsr[p, t]^2/(2 \[Pi] \[Phi]srp[t]))^2
32 nSsr1[t_] := 1 - 4 \[Epsilon]H1[p, t] - 2 \[Delta]H1[p, t]
33 PTsr1[t_] := (1 + (2 \[Alpha] - 2) \[Epsilon]H1[p, t]) (Hsr[p, t]/(
34     2 \[Pi]))^2
35 nTsr1[t_] := -2 \[Epsilon]H1[p, t]
36 (*Second Order*)
37 PSsr2[t_] := (1 + (4 \[Alpha] - 2) \[Epsilon]H1[p, t] +
38     2 \[Alpha] \[Delta]H1[p,
39     t] + (4 \[Alpha]^2 - 23 + 7 \[Pi]^2/3) \[Epsilon]H1[p,
40     t]^2 + (3 \[Alpha]^2 + 2 \[Alpha] - 22 +
41     29 \[Pi]^2/12) \[Epsilon]H1[p, t] \[Delta]H1[p,
42     t] + (3 \[Alpha]^2 - 4 + 5 \[Pi]^2/12) \[Delta]H1[p,
43     t]^2 + (-\[Alpha]^2 + \[Pi]^2/12) \[Delta]H2[p, t]) (Hsr[p,
44     t]^2/(2 \[Pi] \[Phi]srp[t]))^2
45 nSsr2[t_] :=
46 1 - 4 \[Epsilon]H1[p, t] -
47 2 \[Delta]H1[p, t] + (8 \[Alpha] - 8) \[Epsilon]H1[p,
48 t]^2 + (10 \[Alpha] - 6) \[Epsilon]H1[p, t] \[Delta]H1[p, t] -
49 2 \[Alpha] \[Delta]H1[p, t]^2 + 2 \[Alpha] \[Delta]H2[p, t]
50 PTsr2[t_] := (1 + (2 \[Alpha] - 2) \[Epsilon]H1[p,
51 t] + (2 \[Alpha]^2 - 2 \[Alpha] - 3 + \[Pi]^2/2) \[Epsilon]H1[p,
52 t]^2 + (-\[Alpha]^2 + 2 \[Alpha] - 2 + \[Pi]^2/
53 12) \[Epsilon]H2[p, t]) (Hsr[p, t]/(2 \[Pi]))^2
54 nTsr2[t_] := -2 \[Epsilon]H1[p, t] -
55 2 \[Epsilon]H1[p, t]^2 + (2 \[Alpha] - 2) \[Epsilon]H2[p, t]
56 teval[k_] := (t /.
57     First[FindRoot[k == asr[t] (Hsr[p, t]), {t, 10^6}]]])

```

Listing A.7: Code for calculation of perturbations and observables numerically.

```

1 \[Mu] := 20
2 M := Import[

```

```

3      "C:\\Users\\RAUL\\Documents\\Wolfram_Mathematica\\Titulation_\\
4 Cosmology\\data_ex\\mvalues_ex_k005_N60.csv"][[\\[Mu], 2]];
5 p := 4
6 \\[Phi]end := First[cend[p, \\[Mu]]]
7 \\[Phi]ini := First[cini[p, \\[Mu]]]
8 V[t_] := M^4 (1 - (\\[Phi][t]/\\[Mu])^p)
9 Vp[t_] = D[V[t], \\[Phi][t]];
10 ten := 4.57 10^6
11 (*\\[Phi]sr, asr*)
12 sol = NDSolve[{ 3 a'[t]/a[t] \\[Phi]'[t] + Vp[t] == 0,
13               a'[t] == a[t] Sqrt[1/3 (V[t])],
14               \\[Phi][0] == \\[Phi]ini, a[0] == 1}, {\\[Phi], a},
15               {t, -90000, ten}, MaxSteps -> 100000, AccuracyGoal -> 10];
16 \\[Phi]sr[t_] := (\\[Phi] /. First[sol])[t]
17 \\[Phi]srp[t_] = D[\\[Phi]sr[t], {t, 1}];
18 (*\\[Phi], a*)
19 Vt[t_] := M^4 (1 - (\\[Phi]t[t]/\\[Mu])^p)
20 Vtp[t_] = D[Vt[t], \\[Phi]t[t]];
21 sol1 = NDSolve[{\\[Phi]t''[t] + 3 at'[t]/at[t] \\[Phi]t'[t] + Vtp[t] ==
22               0,
23               at'[t] == at[t] Sqrt[1/3 (1/2 \\[Phi]t'[t]^2 + Vt[t])],
24               \\[Phi]t[0] == \\[Phi]sr[0], \\[Phi]t'[0] == \\[Phi]srp[0],
25               at[0] == 1}, {\\[Phi]t, at},
26               {t, -90000, ten}, MaxSteps -> 100000, AccuracyGoal -> 10];
27 \\[Phi]t[t_] := (\\[Phi]t /. First[sol1])[t]
28 p\\[Phi]t[t_] := (\\[Phi]t' /. First[sol1])[t];
29 pp\\[Phi]t[t_] := (\\[Phi]t'' /. First[sol1])[t];
30 ppp\\[Phi]t[t_] := (\\[Phi]t''' /. First[sol1])[t];
31 a[t_] := (at /. First[sol1])[t];
32 pa[t_] := (at' /. First[sol1])[t];
33 ppa[t_] := (at'' /. First[sol1])[t];
34 pppa[t_] := (at''' /. First[sol1])[t];
35 H[t_] := pa[t]/a[t]
36 z[t_] := (a[t] p\\[Phi]t[t])/H[t]
37 tend = t /. FindRoot[\\[Phi]t[t] == \\[Phi]end, {t, ten *0.9}];
38 Efolds = Log[a[tend]/a[0]];
39 pH[t_] = D[H[t], t];
40 z[t_] := ((a[t])^2 p\\[Phi]t[t])/pa[t];

```

```

41 pz[t_] :=
42 a[t] (p\[Phi][t] (2 - (a[t] ppa[t])/pa[t]^2) + (a[t] pp\[Phi][t])/
43 pa[t])
44 ppz[t_] :=
45 2 pa[t] p\[Phi][t] + (2 a[t]^2 p\[Phi][t] ppa[t]^2)/pa[t]^3 +
46 4 a[t] pp\[Phi][t] - (
47 a[t]^2 (2 ppa[t] pp\[Phi][t] + p\[Phi][t] pppa[t]))/pa[t]^2 + (
48 a[t] (-2 p\[Phi][t] ppa[t] + a[t] ppp\[Phi][t]))/pa[t]
49
50 conformal =
51 NDSolve[{conf'[t] == 1/a[t], conf[Re[tend]] == 0}, {conf,
52 conf'}, {t, 0, tend}, AccuracyGoal -> 10, PrecisionGoal -> 10,
53 WorkingPrecision -> 15, MaxSteps -> Infinity,
54 InterpolationOrder -> All];
55 \[Eta][t_] := (conf /. First[conformal])[t];
56 p\[Eta][t_] := (conf' /. First[conformal])[t];
57 rhsScalar[k_, t_] :=
58 1/(a[t])^2 (k^2 - a[t]/z[t] ((pa[t] pz[t]) + (a[t] ppz[t])));
59 rhsTensor[k_, t_] := ((k/a[t])^2 - (pa[t]/a[t])^2 - ppa[t]/a[t]);
60 hc[k_] := Rationalize[FindRoot[k - pa[t], {t, 10^6}][[1, 2]], 0];
61 uini[k_, t_] := Rationalize[Exp[-I k \[Eta][t]]/Sqrt[2 k], 0];
62 diffuini[k_, t_] :=
63 Rationalize[-(Exp[-I k \[Eta][t]]/Sqrt[2 k]) (I k p\[Eta][t]), 0];
64 nzeros[k_] :=
65 n /. First[
66 NSolve[n == Pi^-1 k (\[Eta][hc[k]] - \[Eta][0]), n,
67 WorkingPrecision -> 15]]
68 etabuch[k_] := NSolve[k (\[Eta][hc[k]] - eta) == 500 Pi, eta]
69 etaini[k_] := NSolve[k (\[Eta][hc[k]] - eta) == 300 Pi, eta]
70 suptbuch[k_] :=
71 FindRoot[\[Eta][t] == (eta /. First[etabuch[k]]), {t, 500, 1000}][[1,
72 2]]
73 suptini[k_] :=
74 FindRoot[\[Eta][t] == (eta /. First[etaini[k]]), {t, 500, 1000}][[1,
75 2]]
76 tbuch[k_] :=
77 Piecewise[{{hc[k]*0.001, k <= .06}, {suptbuch[k], k > .06}}];
78 tini[k_] := Piecewise[{{hc[k]*.05, k <= .06}, {suptini[k], k > .06}}]

```

```

79 prere[k_] :=
80   NDSolve[{l''[t] + l'[t] H[t] + l[t] (k/a[t])^2 == 0,
81     l[tbuch[k]] == Re[uini[k, tbuch[k]]],
82     l'[tbuch[k]] == Re[diffuini[k, tbuch[k]]]}, {l, l'}, {t, tbuch[k],
83     tini[k]}, MaxSteps -> Infinity, StartingStepSize -> .0001,
84     MaxStepSize -> 10, InterpolationOrder -> All];
85 re[k_] :=
86   NDSolve[{u''[t] + u'[t] H[t] + u[t] rhsScalar[k, t] == 0,
87     u[tini[k]] == Rationalize[(1 /. First[prere[k]])[tini[k]], 0],
88     u'[tini[k]] == Rationalize[(1' /. First[prere[k]])[tini[k]], 0]},
89     u, {t, tini[k], 3 hc[k]}, MaxSteps -> Infinity,
90     StartingStepSize -> .001, MaxStepSize -> 10,
91     InterpolationOrder -> All];
92 preim[k_] :=
93   NDSolve[{g''[t] + g'[t] H[t] + g[t] (k/a[t])^2 == 0,
94     g[tbuch[k]] == Im[uini[k, tbuch[k]]],
95     g'[tbuch[k]] == Im[diffuini[k, tbuch[k]]]}, {g, g'}, {t, tbuch[k],
96     tini[k]}, MaxSteps -> Infinity, StartingStepSize -> .0001,
97     MaxStepSize -> 10, InterpolationOrder -> All];
98 im[k_] :=
99   NDSolve[{v''[t] + v'[t] H[t] + v[t] rhsScalar[k, t] == 0,
100     v[tini[k]] == Rationalize[(g /. First[preim[k]])[tini[k]], 0],
101     v'[tini[k]] == Rationalize[(g' /. First[preim[k]])[tini[k]], 0]},
102     v, {t, tini[k], 3 hc[k]}, MaxSteps -> Infinity,
103     StartingStepSize -> .001, MaxStepSize -> 10,
104     InterpolationOrder -> All];
105 x[k_] := u /. First[re[k]]
106 y[k_] := v /. First[im[k]]
107 (*Tensor*)
108 prere2[k_] :=
109   NDSolve[{l''[t] + l'[t] H[t] + l[t] (k/a[t])^2 == 0,
110     l[tbuch[k]] == Re[uini[k, tbuch[k]]],
111     l'[tbuch[k]] == Re[diffuini[k, tbuch[k]]]}, {l, l'}, {t, tbuch[k],
112     tini[k]}, MaxSteps -> Infinity, StartingStepSize -> .0001,
113     MaxStepSize -> 10, InterpolationOrder -> All];
114 re2[k_] :=
115   NDSolve[{u''[t] + u'[t] H[t] + u[t] rhsTensor[k, t] == 0,
116     u[tini[k]] == Rationalize[(1 /. First[prere[k]])[tini[k]], 0],

```

```

117     u'[tini[k]] == Rationalize[(1' /. First[prere[k]])[tini[k]], 0]},
118     u, {t, tini[k], 3 hc[k]}, MaxSteps -> Infinity,
119     StartingStepSize -> .001, MaxStepSize -> 10,
120     InterpolationOrder -> All];
121 preim2[k_] :=
122     NDSolve[{g''[t] + g'[t] H[t] + g[t] (k/a[t])^2 == 0,
123     g[tbuch[k]] == Im[uini[k, tbuch[k]]],
124     g'[tbuch[k]] == Im[diffuini[k, tbuch[k]]]}, {g, g'}, {t, tbuch[k],
125     tini[k]}, MaxSteps -> Infinity, StartingStepSize -> .0001,
126     MaxStepSize -> 10, InterpolationOrder -> All];
127 im2[k_] :=
128     NDSolve[{v''[t] + v'[t] H[t] + v[t] rhsTensor[k, t] == 0,
129     v[tini[k]] == Rationalize[(g /. First[preim[k]])[tini[k]], 0],
130     v'[tini[k]] == Rationalize[(g' /. First[preim[k]])[tini[k]], 0]},
131     v, {t, tini[k], 3 hc[k]}, MaxSteps -> Infinity,
132     StartingStepSize -> .001, MaxStepSize -> 10,
133     InterpolationOrder -> All];
134 x2[k_] := u /. First[re2[k]]
135 y2[k_] := v /. First[im2[k]]
136 PS[k_] :=
137     k^3/(2 Pi^2 (z[3 hc[k]])^2) Abs[(x[k])[3 hc[k]] + I (y[k])[3 hc[k]]]^2
138 PT[k_] :=
139     k^3/(2 Pi^2 (a[3 hc[k]])^2)
140     Abs[(x2[k])[3 hc[k]] + I (y2[k])[3 hc[k]]]^2
141 nS[k_] := 1 + k/PS[k] (PS[k + h2] - PS[k - h2])/(2 h2)
142 r[k_] := 8 PT[k]/PS[k]

```

Listing A.8: Code for calculation of fitting of $P_S(k)$.

```

1
2 powerspectra :=
3     Import["C:\\Users\\RAUL\\Documents\\Wolfram_Mathematica\\Titulation_\\
4     _Cosmology\\Approach_fitting_PS\\data_PS\\k_vs_PS(k)_mu=20.dat",
5     "Table"]
6
7 kpivot := 0.05
8
9 fit = NonlinearModelFit[powerspectra,
10     AS (k/kpivot)^(spec - 1 +

```



```
11      1/2 \[Alpha] Log[k/kpivot] + \[Beta]/6 (Log[k/kpivot])^2), {AS,  
12      spec, \[Alpha], \[Beta]}, k  
13  
14 PPS[k_] :=  
15 2.136834395930296'^-9 E^(-0.10542561370312366' -  
16 0.0001685987644504388' Log[20.' k]^2)  
17 k^(-0.036352362643531644' - 0.00038736045818737607' Log[20.' k] -  
18 0.00005627965020065743' Log[20.' k]^2)  
19 dPPS[k_] = D[PPS[k], {k, 1}];  
20 nnS[k_] = 1 + k/PPS[k] dPPS[k];
```


Bibliography

- [1] Planck Collaboration, *et al.* Planck 2018 results - X. Constraints on inflation. *A&A* **2020**, *641*, A10.
- [2] Friedman, A. Über die krümmung des raumes. *Zeitschrift für Physik* **1922**, *10*, 377–386.
- [3] Lopez-Corredoira, M. History and Problems of the Standard Model in Cosmology. *arXiv preprint arXiv:2307.10606* **2023**,
- [4] Hubble, E. A relation between distance and radial velocity among extra-galactic nebulae. *Proceedings of the national academy of sciences* **1929**, *15*, 168–173.
- [5] Lemaître, G. The beginning of the world from the point of view of quantum theory. *Nature* **1931**, *127*, 706–706.
- [6] Friedmann, A. On the Possibility of a world with constant negative curvature of space <https://doi.org/10.1007/BF01328280> *Z.* 1924.
- [7] Robertson, H. P. Kinematics and world-structure. *Astrophysical Journal*, vol. 82, p. 284 **1935**, 82, 284.
- [8] Walker, A. G. On Milne's theory of world-structure. *Proceedings of the London Mathematical Society* **1937**, *2*, 90–127.
- [9] Kundu, S. Single field inflation: observables and constraints. Ph.D. thesis, 2014.
- [10] Weinberg, S. *Cosmology*; OUP Oxford, 2008.
- [11] Lyth, D. H.; Liddle, A. R. *The primordial density perturbation: Cosmology, inflation and the origin of structure*; Cambridge university press, 2009.
- [12] Vazquez Gonzalez, J. A.; Padilla, L. E.; Matos, T. Inflationary cosmology: from theory to observations. *Revista Mexicana de Física E* **2020**, *17*, 73–91.
- [13] Lyth, D. *Cosmology for physicists*; CRC Press, 2016.
- [14] Liddle, A. *An introduction to modern cosmology*; John Wiley & Sons, 2015.
- [15] Roos, M. *Introduction to cosmology*; John Wiley & Sons, 2015.

-
- [16] Guth, A. H. Inflationary universe: A possible solution to the horizon and flatness problems. *Physical Review D* **1981**, *23*, 347.
- [17] Liddle, A. R.; Lyth, D. H. *Cosmological inflation and large-scale structure*; Cambridge university press, 2000.
- [18] Lakhal, B. S.; Guezmir, A. The Horizon Problem. 2019.
- [19] Martin, J. Inflation and precision cosmology. *Brazilian journal of physics* **2004**, *34*, 1307–1321.
- [20] Ryden, B. *Introduction to cosmology*; Cambridge University Press, 2017.
- [21] Brawer, R. Inflationary cosmology and horizon and flatness problems: the mutual constitution of explanation and questions. Ph.D. thesis, Massachusetts Institute of Technology, 1995.
- [22] others,, *et al.* Improved constraints on primordial gravitational waves using Planck, WMAP, and BICEP/Keck observations through the 2018 observing season. *Physical review letters* **2021**, *127*, 151301.
- [23] Di Valentino, E.; Giarè, W.; Melchiorri, A.; Silk, J. Quantifying the global ‘CMB tension’ between the Atacama Cosmology Telescope and the Planck satellite in extended models of cosmology. *Monthly Notices of the Royal Astronomical Society* **2023**, *520*, 210–215.
- [24] Martin, J. Cosmic Inflation: Trick or Treat? *arXiv e-prints* **2019**, arXiv:1902.05286.
- [25] Baumann, D. Cosmology, part iii mathematical tripos. *University lecture notes* **2014**, *56*, 34.
- [26] Mukhanov, V. F. *Physical foundations of cosmology*; Cambridge university press, 2005.
- [27] Coone, D.; Roest, D.; Vennin, V. The Hubble flow of plateau inflation. *Journal of Cosmology and Astroparticle Physics* **2015**, *2015*, 010.
- [28] Liddle, A. R.; Parsons, P.; Barrow, J. D. Formalising the Slow-Roll Approximation in Inflation. *Sussex Preprint* **1994**,
- [29] Boubekeur, L.; Lyth, D. H. Hilltop inflation. *Journal of Cosmology and Astroparticle Physics* **2005**, *2005*, 010.
- [30] Lyth, D. H.; Riotto, A. Particle physics models of inflation and the cosmological density perturbation. *Physics Reports* **1999**, *314*, 1–146.
- [31] Dimopoulos, K. An analytic treatment of quartic hilltop inflation. *Physics Letters B* **2020**, *809*, 135688.
- [32] Tapia, T.; Rojas, C. Scalar Cosmological Perturbations. *arXiv preprint arXiv:2007.04423* **2020**,
- [33] Mukhanov, V. F.; Feldman, H. A.; Brandenberger, R. H. Theory of cosmological perturbations. *Physics reports* **1992**, *215*, 203–333.
- [34] Deruelle, N.; Gundlach, C.; Polarski, D. On the quantization of perturbations in inflation. *Classical and Quantum Gravity* **1992**, *9*, 137–148.

-
- [35] Sriramkumar, L. An introduction to inflation and cosmological perturbation theory. *Current science* **2009**, 868–886.
- [36] Tapia, T.; Mughal, M. Z.; Rojas, C. Semiclassical analysis of the Starobinsky inflationary model. *Physics of the Dark Universe* **2020**, *30*, 100650.
- [37] Habib, S.; Heinen, A.; Heitmann, K.; Jungman, G. Inflationary perturbations and precision cosmology. *Physical Review D* **2005**, *71*, 043518.
- [38] Meza, S.; Altamirano, D.; Mughal, M. Z.; Rojas, C. Numerical analysis of the generalized Starobinsky inflationary model. *International Journal of Modern Physics D* **2021**, *30*, 2150062.
- [39] Giarè, W.; Pan, S.; Valentino, E. D.; Yang, W.; de Haro, J.; Melchiorri, A. Inflationary potential as seen from different angles: model compatibility from multiple CMB missions. *Journal of Cosmology and Astroparticle Physics* **2023**, *2023*, 019.
- [40] Martin, J.; Ringeval, C.; Vennin, V. Encyclopædia inflationaris. *Physics of the Dark Universe* **2014**, *5*, 75–235.
- [41] Wolfram Research, Inc., Mathematica, Versión 13.3. <https://www.wolfram.com/mathematica>.